Comprehensive DFT Study of Nitrous Oxide Decomposition over Fe-ZSM-5†

Andreas Heyden,*,‡ Baron Peters,§ Alexis T. Bell,*,§ and Frerich J. Keil‡

Department of Chemical Engineering, Hamburg University of Technology, D-21073 Hamburg, Germany, and Department of Chemical Engineering, University of California, Berkeley, California 94720-1462

Received: August 13, 2004; In Final Form: November 10, 2004

The reaction mechanism for nitrous oxide decomposition has been studied on hydrated and dehydrated mononuclear iron sites in Fe−ZSM-5 using density functional theory. In total, 46 different surface species with different spin states (spin multiplicity $M_S = 4$ or 6) and 63 elementary reactions were considered. Heats of adsorption, activation barriers, reaction rates, and minimum energy pathways were determined. The approximate minimum energy pathways and transition states were calculated using the "growing string method" and a modified "dimer method". Spin surface crossing (e.g., O_2 desorption) was considered. The minimum potential energy structure on the seam of two potential energy surfaces was determined with a multiplier penalty function algorithm by Powell and approximate rates of spin surface crossings were calculated. It was found that nitrous oxide decomposition is first order with respect to nitrous oxide concentration and zero order with respect to oxygen concentration. Water impurities in the gas stream have a strong inhibiting effect. In the concentration range of 1−100 ppb, the presence of water vapor influences the surface composition and the apparent rate coefficient. This is especially relevant in the temperature range of 600−700 K where most experimental kinetic studies are performed. Apparent activation barriers determined over this temperature range vary from 28.4 (1 ppb H_2O) to 54.8 kcal/mol (100 ppb H_2O). These results give an explanation why different research groups and different catalyst pretreatments often result in very different activation barriers and preexponential factors. Altogether perfect agreement with experimental results could be achieved.

Introduction

Iron-exchanged ZSM-5 is an active catalyst for the stoichiometric decomposition of N_2O to N_2 and O_2[1−11] and is therefore a potentially useful material for the removal of N_2O, a molecule with a high greenhouse potential, from industrial waste streams. These findings have stimulated an interest in identifying the nature of the active site for nitrous oxide decomposition and the mechanism via which this reaction occurs.

The state of iron in Fe−ZSM-5 is strongly dependent on the method of iron exchange, the level of Fe exchange (i.e., the Fe/Al ratio), and the pretreatment of the as-exchanged material. EXAFS characterization of Fe−ZSM-5 prepared by aqueous ion exchange of H−ZSM-5 conducted by Joyner and Stockenhuber[12] showed the presence of isolated iron cations, large clusters of Fe_3O_4, as well as Fe_4O_4 nanoclusters. The disordered nature of the abundantly present iron oxide aggregates and the possibility of a minority species responsible for catalysis have been reported more recently by van Santen and co-workers.[13,14] Careful preparation of Fe−ZSM-5 by dry exchange of H−ZSM-5 minimizes the formation of Fe_3O_4 and enhances the dispersion of Fe as well-defined species. EXAFS data by Battiston et al.,[15−18] Marturano et al.,[19,20] and Jia et al.[21] of fully exchanged H−ZSM-5 (Fe/Al = 1) shows evidence for diferric oxo/hydroxyl-bridged clusters. Marturano et al.[19] have also shown that the distribution of iron in Fe−ZSM-5 is strongly dependent on the source of the parent ZSM-5 and have noted that, with some ZSM-5 samples, particles of Fe_2O_3 can form after calcination of the as-exchanged material. Mössbauer spectroscopy has also been used to provide evidence for di-iron sites in studies reported by Dubkov et al.[22] On the other hand, Perez-Ramirez et al.[23] have observed isolated iron cations and small oligonuclear oxo-iron complexes in the zeolite channels by Mössbauer spectroscopy and voltammetry. Overweg et al.[24] concluded from ^{57}Fe Mössbauer data that there cannot be a similarity between the active Fe species and the binuclear clusters in methane monooxygenase (MMO) as claimed by Dubkov et al.[22]

Evidence for isolated Fe sites in partially exchanged samples of ZSM-5 has been obtained in several recent studies. Lobree et al.[25] and similarly Kucherov and Shelef[26] have reported that, for Fe/Al ratios below ∼ 0.6, Fe^{3+} cations exchange on a one to one basis with Brønsted acid protons in H−ZSM-5. EXAFS analyses conducted by Choi et al.[27,28] have confirmed that for Fe/Al < 1.0 isolated Fe^{3+} cations associated with single charge-exchange sites are present in Fe−ZSM-5 prepared by solid-state exchange of H−ZSM-5 with $FeCl_3$ and by high-temperature pretreatment of Fe/Al-MFI. In a related work, Perez-Ramirez et al.[29] have demonstrated that isolated iron ions in extraframework positions have the highest activity per mole of iron.

Several quantum chemical studies have been reported aimed at identifying the mechanism by which N_2O decomposes to form N_2 and O_2. Zhidomirov and co-workers[30,31] have investigated the decomposition of N_2O on an active single iron site modeled as $Fe(OH)_3(H_2O)_2$ and on an Fe^{2+} ion stabilized by interaction with four oxygen atoms from two intersecting five-membered zeolite rings. These authors have also investigated N_2O decomposition on binuclear Fe complexes in ZSM-5.[32] In the study, the zeolite was represented by a pair of 5T rings sharing an edge and the Fe complex was represented as either $[(HO)FeOFe(OH)]^{2+}$ or $[FeOFe]^{2+}$. Neither activation energies nor rates of

† Dedicated to Prof. Gerhard Ertl on the occasion of his retirement as a director of the Fritz-Haber-Institut of the Max-Planck-Gesellschaft in Berlin.

* To whom correspondence should be addressed. E-mail: a.heyden@tuhh.de (A.H.); bell@cchem.berkeley.edu (A.T.B.).

‡Hamburg University of Technology.

§ University of California, Berkeley.

10.1021/jp040549a CCC: $30.25
Published on Web 01/19/2005

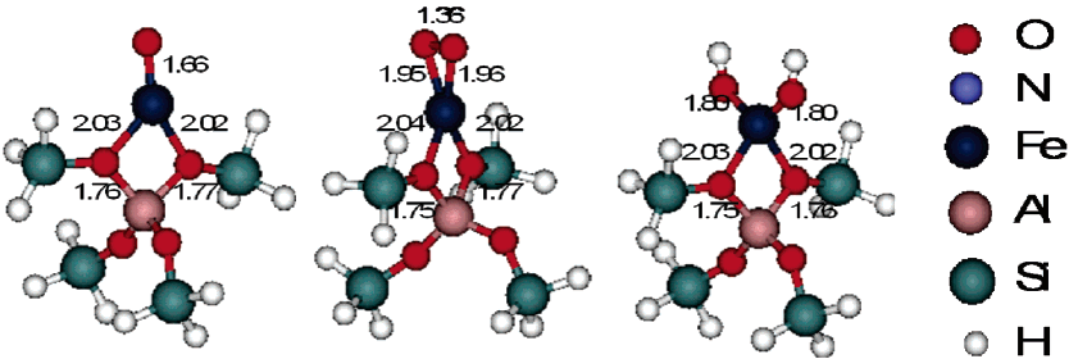

Figure 1. Iron oxo/hydroxo zeolite cluster of most abundant surface species. Structures are potential energy minima on the potential energy surface with spin multiplicity $M_S = 6$. Left: Active site for N_2O decomposition. Middle: Possible α-oxygen site. Right: Deactivated iron hydroxo site. Atomic distances in angstroms are indicated.

N_2O decomposition were reported in the latter two studies. Yoshizawa et al.[33,34] investigated the decomposition of N_2O on mononuclear iron sites. In their study, a fully relaxed 3T cluster with a bare iron site $Z^-[Fe]^+$ was used. An activation energy of 2.4 kcal/mol was calculated for the decomposition of N_2O. Ryder et al.[35] investigated the full cycle of the N_2O decomposition on a constrained 5T zeolite cluster $Z^-[FeO]^+$. Although their calculated apparent activation energy is in reasonable agreement with experiments, the value of the preexponental factor is an order of magnitude smaller than that observed.

The purpose of the present study is to analyze the energetics and kinetics of the nitrous oxide decomposition on hydrated and dehydrated mononuclear iron sites in Fe−ZSM-5. The active site and a small portion of the zeolite were described as a cluster. Following the work from Yoshizawa et al.[34,38] and Shaik et al.,[39−41] who proposed that more than one state should be involved in the reactions catalyzed by organometallic systems ("two-state reactivity"), we analyzed multiple spin states and calculated approximate rates of spin surface crossing. The minimum potential energy structure on the seam of two potential energy surfaces was determined with a multiplier penalty function algorithm taken from Powell.[42] This approach enabled calculation of the rate of O_2 desorption. The "growing string method"[43] and a modified "dimer method"[44] were used to calculate transition states and approximate minimum energy pathways. These methods accelerated the search for transition states dramatically and guaranteed that the transition state was connected to the expected reactant and product states. In contrast to other transition state search algorithms, the growing string method does not require a priori assumptions about the reaction pathway.

An important part of the investigation was the determination of the effects of low concentrations of water on speciation of Fe in Fe−ZSM-5. This part of the investigation was stimulated by the work of Wood et al.[36] and Kiwi-Minsker et al.,[11,37] who proposed that low concentrations of water vapor could alter the concentration of active Fe species. The mechanism and rate parameters obtained from the present study were used to simulate the overall kinetics of N_2O decomposition and were found to describe correctly the apparent activation barrier and preexponential factor reported by a number of authors. The role of trace amounts of water vapor on the apparent activation energy and preexponential factor were also identified.

Theory

The catalytically active center and a portion of the zeolite framework are represented by a 23−27 atom cluster. As shown in Figure 1, the portion of the cluster describing the zeolite contains an Al atom in the T12 site of the framework surrounded by shells of O and Si atoms. The terminal Si atoms are fixed in their crystallographic positions as reported by Olson et al.[45] Dangling bonds are terminated by H atoms located 1.5 Å from each terminal Si atom oriented in the direction of the next T (tetrahedral) site. The anionic cluster is charge-compensated by a metal-oxo species, $[Fe]^+$, $[FeO]^+$, $[FeO_2]^+$, $[OFeO]^+$, $[O_2FeO]^+$, $[O_2FeO_2]^+$, $[Fe(OH)_2]^+$, $[OFe(OH)_2]^+$, or $[O_2Fe(OH)_2]^+$, placed between two of the four O atoms surrounding the Al atom.

Quantum chemical calculations of the geometry and energies of potential energy minima, transition-state structures, and minimum energy structures on the seam of two PES were performed for multiple spin surfaces (i.e., spin multiplicity $M_S = 4$ and 6), using nonlocal, gradient-corrected density-functional theory (DFT).[46] PES minima were also calculated for $M_S = 2$ and 8. To represent the effects of exchange and correlation, Becke's 3-parameter exchange functional and the correlation functional of Lee, Yang, and Parr (B3LYP) were used with a very fine grid size.[47,48] Basis sets at the triple-ζ level with polarization functions were used for all atoms, including Fe (TZVP).[49] No corrections were made for basis set superposition error (BSSE).[50] All calculations and reported values were carried out using the TURBOMOLE V5.6 suite of programs.[51,52]

Calculations on different spin surfaces revealed that only the PESs with spin multiplicity $M_S = 4$ and 6 need to be considered. Consequently, just these results are reported. Spin contamination was negligible for ground-state structures on the spin surface $M_S = 6$. Some spin contamination was observed for transition states, minimum structures on a seam of two PES, and minimum energy structures on the $M_S = 4$ surface. In all cases, it was still possible to distinguish clearly between states of different spin multiplicities. Following the work of Zilberberg et al.,[53] who showed that despite some spin contamination the relative energies and geometry of different states of $OFe(OH)_2$ calculated with DFT-B3LYP are in good agreement with predictions of CASSCF-MCQDPT2 calculations, we concluded that a DFT-B3LYP approach could also be used successfully for the present studies.

Additional modules were programmed to extend the functionality of the TURBOMOLE V5.6 program package for finding transition states and minimum energy structures on the seam of two PES. In the following, we briefly explain the functionality of these modules.

TURBOMOLE V5.6 does not allow fixing specific atoms in a molecule cluster. We changed the TURBOMOLE V5.6 optimization script, set the Cartesian gradient component of fixed atoms to zero, and reset the coordinates of every fixed

atom after each cycle. Fast convergence properties were observed for minimizations with an energy convergence criterion of at least 10^{-7} Ha and a gradient norm convergence criterion of 10^{-4} Ha/bohr. At the end of all minimizations or saddle point searches, a frequency calculation was done to confirm that for minima all frequencies are positive and for saddle points exactly one frequency is imaginary. To account correctly for the fixed atoms in a frequency calculation, the components of the fixed atoms are carved out of the Cartesian second derivative matrix. Afterward, the frequencies of this reduced Hessian are calculated.[54]

To accelerate the search for transition states, a combination of interpolation and local methods was used. The "growing string method"[43] was used to find an approximation to the transition state, since this method has been reported to be superior to the nudged elastic band[55,56] and other string methods.[57] The "growing string method" was used in mass-weighted coordinates with a maximum of 11 to 15 nodes. After the two separate ends join, the "growing string method" was terminated and an approximate saddle point was obtained. To refine the position of the saddle point, the modified "dimer method"[44] was employed. A convergence criterion of the gradient norm of 5×10^{-4} Ha/bohr was used for transition states, and as described above, first-order saddle points were identified with a frequency calculation. Owing to the use of mass-weighted coordinates in the "growing string method" an approximation to the minimum energy path (MEP) was obtained, which could be used to determine that reactant and product states are linked by the transition structure found.

The minimum potential energy structure on the seam of two potential energy surfaces was determined with a multiplier penalty function algorithm by Powell.[42] The function F was minimized

$$F(R;M_{Si},M_{Sj},\lambda,\mu) = E(R,M_{Si}) + E(R,M_{Sj}) - \lambda\cdot(E(R,M_{Si}) - E(R,M_{Sj})) + \frac{1}{2}\mu(E(R,M_{Si}) - E(R,M_{Sj}))^2 \quad (1)$$

for the coordinates R with fixed parameters M_{Si}, M_{Sj}, λ and μ using the quasi-Newton algorithm of Broyden, Fletcher, Goldfarb, and Shanno (BFGS).[58] M_{Si} and M_{Sj} are the spin multiplicities, λ is the Lagrange multiplier, and μ is the penalty function parameter. When the energy of the structure on the two PES differs by less than 75% between two minimizations the Lagrange multiplier λ is updated

$$\lambda^{k+1} = \lambda^k - \mu(E(R,M_{Si}) - E(R,M_{Sj})) \quad (2)$$

Otherwise, the penalty function parameter μ is multiplied by 10. The optimization is repeated with the updated parameters until the minimization results in an energy difference of the structure on the two PESs of 10^{-6} Ha. After every constrained minimization, the second derivative matrix H of the electronic energy was calculated on both PES (as described above). To confirm that the optimized structure is a minimum on the seam of two PES, we projected the vector υ

$$\upsilon = \mathrm{grad}(E(R,M_{Si})) - \mathrm{grad}(E(R,M_{Sj})) \quad (3)$$

out of the matrix $\nabla_x^2 L$

$$\nabla_x^2 L = H(R,M_{Si})(1-\lambda) + H(R,M_{Sj})(1+\lambda) \quad (4)$$

and verified that the eigenvalues of this projected matrix are all positive.[58]

Overall equilibrium constants and reaction rate constants were computed using standard statistical mechanics and absolute rate theory.[59] We used the harmonic approximation, and included the contributions of the translational, rotational, vibrational, and electronic partition functions of all gaseous species participating in the reaction and the vibrational and electronic contribution of the zeolite cluster. Since the zeolite cluster is part of a solid, translational and rotational partition functions for the zeolite were assumed to be equal in the reactant and transition state. The procedure described above is not able to determine rates of spin−surface crossing. The minimum-energy structure on the seam of two PES is not a stationary point. Since the species with low spin multiplicity in our work is usually an adsorbed species (e.g., adsorbed O_2), the framework of absolute rate theory is used under the assumption that the partition functions of the hypothetical transition state (minimum on the seam of two PES) and the reactant state (minimum on PES with lower spin multiplicity) are identical. Consequently

$$k_{low\rightarrow high} = \frac{k_B T}{h}\exp\left(-\frac{\Delta E}{k_B T}\right); \quad k_{high\rightarrow low} = k_{low\rightarrow high}K_{equil} \quad (5)$$

where ΔE is the difference in the electronic energy of the minimum on the seam of the two PES and the reactant state. This corresponds to an energy barrier of ΔE and an escape attempt probability of $k_B T/h$. The same approach was used for rates of desorption on one PES when the adsorption process is barrierless.[60]

It is recognized that for an exact treatment of spin−surface crossing, spin−orbit coupling energies have to be calculated. However, in view of the computational expenses necessary for these calculations the adiabatic approximation was used and spin−orbit coupling was not considered. As a result, the error in the rates of spin−surface crossing can be significantly larger than the error in calculated rates of reaction on one PES. To estimate, if low spin inversion probabilities could result in a significant reduction of the rates of spin−surface crossing, thermally averaged spin transition probabilities are calculated with the Landau−Zener formula[61−64]

$$\bar{P}_{12} = \int_0^\infty \mathrm{d}\upsilon \left(1 - \exp\left\{-\frac{4\pi^2 {H_{12}}^2}{h\upsilon||\mathrm{grad}(E_1) - \mathrm{grad}(E_2)||}\right\}\right) \frac{\exp(-\upsilon^2/2k_B T)}{\int_0^\infty \mathrm{d}\upsilon \exp(-\upsilon^2/2k_B T)} \quad (6)$$

where H_{12} is the spin−orbit coupling energy, υ is the mass-weighted velocity of the system at the crossing point, and $||\mathrm{grad}(E_1) - \mathrm{grad}(E_2)||$ is the absolute value of the mass-weighted difference in directional derivatives perpendicular to the seam at the point of crossing. Here, it is supposed that the velocity of the system is at the crossing point Boltzmann distributed.[64] The spin−orbit coupling energies are assumed to be in the range between 395 and 825 J/mol, as calculated by Danovich and Shaik[65] for the oxidative activation of H_2 by FeO^+. The transmission coefficient for spin inversion can be calculated in our cases as[64]

$$\kappa = 2\bar{P}_{12} - {\bar{P}_{12}}^2 \quad (7)$$

It is important to note that the necessary correction for the reaction rates, owing to a spin inversion probability smaller one, is comparable to the error inherent in the DFT calculations of activation energies. In addition, the rates of spin−surface

crossing were never rate limiting in this work, and hence, spin−surface crossing should not have an influence on the overall kinetics of the reaction network studied.

Results and Discussion

The decomposition of N_2O on a mononuclear iron oxo/hydroxo site can be envisioned to proceed via the following sequence of steps:

$$Z^-[M]^+ + N_2O(g) \leftrightarrow Z^-[M]^+(ON_2) \quad (1)$$

$$Z^-[M]^+(ON_2) \leftrightarrow Z^-[MO]^+ + N_2(g) \quad (2)$$

$$Z^-[MO]^+ + N_2O(g) \leftrightarrow Z^-[MO]^+(ON_2) \quad (3)$$

$$Z^-[MO]^+(ON_2) \leftrightarrow Z^-[M]^+(O_2) + N_2(g) \quad (4)$$

$$Z^-[M]^+(O_2) \leftrightarrow Z^-[M]^+ + O_2(g) \quad (5)$$

In this sequence, $[M]^+$ represents either $[Fe]^+$, $[FeO]^+$, $[FeO_2]^+$, or $[Fe(OH)_2]^+$. Reactions 1 and 3 involve the adsorption of gas-phase N_2O from its O end. Reactions 2 and 4 describe the dissociation of adsorbed N_2O to give N_2 and an adsorbed O atom. Reaction 5 represents the desorption of molecular O_2. The sum of these five steps constitutes a complete catalytic cycle. In what follows, first the calculations on the energetics and structures for a complete catalytic cycle on all three mononuclear iron oxo sites are presented. Then the consequences of water adsorption are demonstrated and the calculations of the energetics and structures for the catalytic cycle on a mononuclear iron hydroxo site presented. For all cases, the results for the PESs with spin multiplicity $M_S = 4$ and 6 are given. All quantum chemical calculations are summarized in Table 1. Thermally averaged Landau−Zener transition probabilities are summarized for a spin−orbit coupling energy of 395 and 825 J/mol for several temperatures in Table 2. All spin inversion transmission coefficients are larger than 0.05. As a result, not correcting reaction rates for spin inversion probabilities smaller one creates errors smaller than an error in the activation barrier of 4 kcal/mol (at 700 K).

Catalytic Cycle on $Z^-[Fe]^+$. Yoshizawa et al.[33,34] have proposed that bare iron sites ($Z^-[Fe]^+$) are responsible for N_2O decomposition. The catalytic cycle on $Z^-[Fe]^+$ is illustrated in Figure 2 for the quartet PES and in Figure 3 for the sextet PES. N_2O adsorbs from the N end with an enthalpy of adsorption of $\Delta H_{ads}(M_S = 4) = -21.8$ kcal/mol or $\Delta H_{ads}(M_S = 6) = -13.3$ kcal/mol (see Table 1a and c). The large difference in the enthalpy of adsorption on both spin surfaces follows from the fact that N_2O cannot adsorb linearly on the sextet surface as it does on the quartet surface. Until a N_2O molecule gets closer than 2.5 Å to the iron atom, the electron configuration of the iron is on the sextet surface $4s^1\,3d^6$ and we have Pauli repulsion. For the nitrous oxide to adsorb, the electron configurations of iron and N_2O have to change. N_2O adsorbs bent on the sextet surface. The N−N−O angle is 133.7° and the N−N bond distance increases from 1.12 to 1.23 Å. The adsorption process on both spin surfaces is barrierless and both adsorption and desorption are rapid. The zero-point-corrected energy of bare iron sites is nearly identical on the quartet and sextet PESs, and the spin change barrier is approximately $E^‡ = 0.3$ kcal/mol. As a result, if bare iron sites are present, both spin states of iron would be populated and N_2O would preferentially adsorb through the N end on the $M_S = 4$ surface. N_2O should not adsorb through its O end, $\Delta H_{ads}(M_S = 6) = 1.9$ kcal/mol, but if N_2O approaches a bare iron site from its O end, the site can be oxidized readily. An activation barrier does not exist for $M_S = 4$, $E^‡ = 0$ kcal/mol, and is very low for $M_S = 6$, $E^‡ = 2.8$ kcal/mol (compared to 2.4 kcal/mol from Yoshizawa et al.[33]). The imaginary frequency associated with the transition state mode is $220i$ cm^{-1} ($M_S = 6$). The major difference between the transition state and the adsorbed state is the bending of the N−N′−O″ bond angle from 180° in the adsorbed state to 162.9° in the transition state. In the product state, the surface oxygen is located 1.68 Å ($M_S = 4$) or 1.66 Å ($M_S = 6$) apart from the Fe atom. The calculated vibrational mode associated with the Fe−O stretch in $Z^-[FeO]^+$ is 700 cm^{-1} on the quartet PES and 878 cm^{-1} on the sextet PES. Taking into account that the enthalpy of reaction is $\Delta H_R(M_S = 4) = -62.2$ kcal/mol or $\Delta H_R(M_S = 6) = -67.9$ kcal/mol, it follows that the reverse reaction is very slow. As a result, bare iron sites are unlikely to exist under reaction conditions in the presence of N_2O. It is worthwhile noting that for bare iron sites the quartet PES ($M_S = 4$) is preferred to the sextet PES ($M_S = 6$), but for oxidized mononuclear iron $Z^-[FeO]^+$, the reverse is true.

$Z^-[FeO]^+$ sites are also catalytically active for N_2O dissociation. N_2O adsorbs from the N end in a barrierless fashion with an enthalpy of adsorption of $\Delta H_{ads}(M_S = 4) = -7.5$ kcal/mol or $\Delta H_{ads}(M_S = 6) = -10.1$ kcal/mol. The zero-point corrected energy of $Z^-[FeO]^+$ in the sextet state is 3.6 kcal/mol lower than in the quartet state. Since the barrier for transition from the sextet to the quartet state is 6.9 kcal/mol, both spin surfaces should be populated under reaction conditions, but the sextet state should dominate. N_2O adsorption from the O end is weaker than from the N end: $\Delta H_{ads}(M_S = 4) = -1.0$ kcal/mol or $\Delta H_{ads}(M_S = 6) = -4.8$ kcal/mol.

Two reaction pathways for N_2O dissociation from $Z^-[FeO]^+(ON_2)$ sites were found on the quartet and sextet PESs. One reaction pathway leads to $Z^-[FeO_2]^+$ in which the two O atoms form either a superoxide O_2^- or a peroxide O_2^{2-} anion attached to an Fe^{2+} or Fe^{3+} cation. The other reaction path leads to a dioxo $Z^-[OFeO]^+$ species. In this section, just the reaction pathway leading to $Z^-[FeO_2]^+$ is discussed. The second pathway is considered in the context of the catalytic cycle occurring on $Z^-[FeO]^+$. The transition state from $Z^-[FeO]^+(ON_2)$ to $Z^-[FeO_2]^+$ is characterized by a bending of the N_2O molecule from 180° in the adsorbed state to 139.8° ($M_S = 4$)/144.5° ($M_S = 6$) in the transition state. In addition, the N′−O″ bond length of the N_2O molecule is increased from 1.20 to 1.45 Å ($M_S = 4$) or 1.56 Å ($M_S = 6$) in the transition state. The activation barrier for the decomposition is $E^‡(M_S = 4) = 29.0$ kcal/mol or $E^‡(M_S = 6) = 30.4$ kcal/mol. The imaginary frequency associated with the transition state mode is $864i$ cm^{-1} ($M_S = 4$) or $825i$ cm^{-1} ($M_S = 6$). Since the enthalpy of reaction of $\Delta H_R(M_S = 4) = -25.7$ kcal/mol or $\Delta H_R(M_S = 6) = -20.0$ kcal/mol, the reverse reaction has a very high barrier and should not occur readily. Ryder et al.[35] found for the same reaction an activation barrier with respect to the gas phase of 31.0 kcal/mol. The agreement with the value of 24.0 kcal/mol (on the sextet PES) calculated in this work is reasonable (see Figure 3), considering that different basis sets and different quantum packages were used in the two studies.

Figure 2 illustrates that the zero-point corrected energy of $Z^-[FeO_2]^+$ on the quartet PES is approximately 2 kcal/mol higher than on the sextet PES. Since the barrier for the transition from the sextet to the quartet state of this species is 5 kcal/mol, both states are populated with a small preference for the sextet state. The O−O bond length in the $Z^-[FeO_2]^+$ species is calculated to be 1.40 Å ($M_S = 4$) or 1.36 Å ($M_S = 6$). The

TABLE 1: Computed Rate Parameters for the Elementary Steps in Nitrous Oxide Dissociation in Fe-ZSM-5[a]

reaction	$E^{\ddagger}$, ΔH^{b} kcal/mol	constant	*T*, K 600	700	800
Part a					
1. $Z^-[Fe]^+ \{M=4\} + N_2O\ (g) \leftrightarrow Z^-[Fe]^+(N_2O)\ \{M=4\}$	$\Delta H_1 = -21.8$	K_1, bar^{-1}	6.35E+01	4.57E+00	6.54E−01
	$E_1^{\ddagger} = 0.0$	A_1, $s^{-1}\ bar^{-1}$	2.54E+06	3.49E+06	4.64E+06
		k_1, $s^{-1}\ bar^{-1}$	2.54E+06	3.49E+06	4.64E+06
	$E_{-1}^{\ddagger} = 23.1$	A_{-1}, s^{-1}	1.25E+13	1.46E+13	1.67E+13
		k_{-1}, s^{-1}	4.01E+04	7.64E+05	7.10E+06
2. $Z^-[FeO]^+ \{M=4\} + N_2O\ (g) \leftrightarrow Z^-[FeO]^+(N_2O)\ \{M=4\}$	$\Delta H_2 = -7.5$	K_2, bar^{-1}	5.15E−05	2.06E−05	1.06E−05
	$E_2^{\ddagger} = 0.0$	A_2, $s^{-1}\ bar^{-1}$	5.71E+05	7.28E+05	9.11E+05
		k_2, $s^{-1}\ bar^{-1}$	5.71E+05	7.28E+05	9.11E+05
	$E_{-2}^{\ddagger} = 8.4$	A_{-2}, s^{-1}	1.25E+13	1.46E+13	1.67E+13
		k_{-2}, s^{-1}	1.11E+10	3.53E+10	8.56E+10
3. $Z^-[FeO_2]^+ \{M=4\} + N_2O\ (g) \leftrightarrow Z^-[FeO_2]^+(N_2O)\ \{M=4\}$	$\Delta H_3 = 0.3$	K_3, bar^{-1}	6.70E−05	6.84E−05	7.14E−05
	$E_3^{\ddagger} = 0.0$	A_3, $s^{-1}\ bar^{-1}$	2.30E+08	3.30E+08	4.52E+08
		k_3, $s^{-1}\ bar^{-1}$	2.30E+08	3.30E+08	4.52E+08
	$E_{-3}^{\ddagger} = 1.5$	A_{-3}, s^{-1}	1.25E+13	1.46E+13	1.67E+13
		k_{-3}, s^{-1}	3.44E+12	4.82E+12	6.33E+12
4. $Z^-[OFeO]^+ \{M=4\} + N_2O\ (g) \leftrightarrow Z^-[OFeO]^+(N_2O)\ \{M=4\}$	$\Delta H_4 = 4.5$	K_4, bar^{-1}	3.54E−08	5.95E−08	9.04E−08
	$E_4^{\ddagger} = 2.8$	A_4, $s^{-1}\ bar^{-1}$	4.57E+06	6.42E+06	8.68E+06
		k_4, $s^{-1}\ bar^{-1}$	4.43E+05	8.68E+05	1.51E+06
	$E_{-4}^{\ddagger} = 0.0$	A_{-4}, s^{-1}	1.25E+13	1.46E+13	1.67E+13
		k_{-4}, s^{-1}	1.25E+13	1.46E+13	1.67E+13
5. $Z^-[O_2FeO]^+ \{M=4\} + N_2O\ (g) \leftrightarrow Z^-[O_2FeO]^+(N_2O)\ \{M=4\}$	$\Delta H_5 = 0.7$	K_5, bar^{-1}	4.63E−07	4.96E−07	5.37E−07
	$E_5^{\ddagger} = 0.0$	A_5, $s^{-1}\ bar^{-1}$	3.36E+06	4.54E+06	5.95E+06
		k_5, $s^{-1}\ bar^{-1}$	3.36E+06	4.54E+06	5.95E+06
	$E_{-5}^{\ddagger} = 0.6$	A_{-5}, s^{-1}	1.25E+13	1.46E+13	1.67E+13
		k_{-5}, s^{-1}	7.26E+12	9.15E+12	1.11E+13
6. $Z^-[Fe(OH)_2]^+ \{M=4\} + N_2O\ (g) \leftrightarrow Z^-[Fe(OH)_2]^+(N_2O)\ \{M=4\}$	$\Delta H_6 = -0.2$	K_6, bar^{-1}	2.30E−04	2.21E−04	2.20E−04
	$E_6^{\ddagger} = 0.0$	A_6, $s^{-1}\ bar^{-1}$	6.30E+08	8.77E+08	1.17E+09
		k_6, $s^{-1}\ bar^{-1}$	6.30E+08	8.77E+08	1.17E+09
	$E_{-6}^{\ddagger} = 1.8$	A_{-6}, s^{-1}	1.25E+13	1.46E+13	1.67E+13
		k_{-6}, s^{-1}	2.74E+12	3.97E+12	5.33E+12
7. $Z^-[OFe(OH)_2]^+ \{M=4\} + N_2O\ (g) \leftrightarrow Z^-[OFe(OH)_2]^+(N_2O)\ \{M=4\}$	$\Delta H_7 = -5.5$	K_7, bar^{-1}	1.64E−03	8.34E−04	5.13E−04
	$E_7^{\ddagger} = 0.0$	A_7, $s^{-1}\ bar^{-1}$	1.13E+08	1.41E+08	1.73E+08
		k_7, $s^{-1}\ bar^{-1}$	1.13E+08	1.41E+08	1.73E+08
	$E_{-7}^{\ddagger} = 6.2$	A_{-7}, s^{-1}	1.25E+13	1.46E+13	1.67E+13
		k_{-7}, s^{-1}	6.89E+10	1.69E+11	3.37E+11
Part b					
8. $Z^-[Fe]^+ \{M=4\} + N_2O\ (g) \leftrightarrow Z^-[FeO]^+ \{M=4\} + N_2\ (g)$	$\Delta H_8 = -62.2$	K_8, −	1.61E+23	9.29E+19	3.49E+17
	$E_8^{\ddagger} = 0.0$	A_8, $s^{-1}\ bar^{-1}$	7.25E+04	3.81E+04	2.26E+04
		k_8, $s^{-1}\ bar^{-1}$	7.25E+04	3.81E+04	2.26E+04
	$E_{-8}^{\ddagger} = 63.6$	A_{-8}, $s^{-1}\ bar^{-1}$	6.80E+04	3.02E+04	1.57E+04
		k_{-8}, $s^{-1}\ bar^{-1}$	4.50E−19	4.10E−16	6.48E−14
9. $Z^-[FeO]^+ \{M=4\} + N_2O\ (g) \leftrightarrow Z^-[FeO]^+(ON_2)\ \{M=4\}$	$\Delta H_9 = -1.0$	K_9, bar^{-1}	9.12E−06	7.92E−06	7.32E−06
	$E_9^{\ddagger} = 0.0$	A_9, $s^{-1}\ bar^{-1}$	1.16E+07	1.63E+07	2.20E+07
		k_9, $s^{-1}\ bar^{-1}$	1.16E+07	1.63E+07	2.20E+07
	$E_{-9}^{\ddagger} = 2.7$	A_{-9}, s^{-1}	1.25E+13	1.46E+13	1.67E+13
		k_{-9}, s^{-1}	1.28E+12	2.06E+12	3.01E+12
10. $Z^-[FeO_2]^+ \{M=4\} + N_2O\ (g) \leftrightarrow Z^-[FeO_2]^+(ON_2)\ \{M=4\}$	$\Delta H_{10} = 0.7$	K_{10}, bar^{-1}	4.52E−06	4.85E−06	5.25E−06
	$E_{10}^{\ddagger} = 0.0$	A_{10}, $s^{-1}\ bar^{-1}$	1.91E+07	2.79E+07	3.88E+07
		k_{10}, $s^{-1}\ bar^{-1}$	1.91E+07	2.79E+07	3.88E+07
	$E_{-10}^{\ddagger} = 1.3$	A_{-10}, s^{-1}	1.25E+13	1.46E+13	1.67E+13
		k_{-10}, s^{-1}	4.22E+12	5.75E+12	7.38E+12
11. $Z^-[OFeO]^+ \{M=4\} + N_2O\ (g) \leftrightarrow Z^-[OFeO]^+(ON_2)\ \{M=4\}$	$\Delta H_{11} = 4.5$	K_{11}, bar^{-1}	1.60E−08	2.69E−08	4.09E−08
	$E_{11}^{\ddagger} = 2.8$	A_{11}, $s^{-1}\ bar^{-1}$	2.08E+06	2.92E+06	3.95E+06
		k_{11}, $s^{-1}\ bar^{-1}$	2.00E+05	3.92E+05	6.83E+05
	$E_{-11}^{\ddagger} = 0.0$	A_{-11}, s^{-1}	1.25E+13	1.46E+13	1.67E+13
		k_{-11}, s^{-1}	1.25E+13	1.46E+13	1.67E+13
12. $Z^-[O_2FeO]^+ \{M=4\} + N_2O\ (g) \leftrightarrow Z^-[O_2FeO]^+(ON_2)\ \{M=4\}$	$\Delta H_{12} = -0.2$	K_{12}, bar^{-1}	7.24E−07	6.95E−07	6.92E−07
	$E_{12}^{\ddagger} = 0.0$	A_{12}, $s^{-1}\ bar^{-1}$	2.33E+06	3.16E+06	4.16E+06
		k_{12}, $s^{-1}\ bar^{-1}$	2.33E+06	3.16E+06	4.16E+06
	$E_{-12}^{\ddagger} = 1.6$	A_{-12}, s^{-1}	1.25E+13	1.46E+13	1.67E+13
		k_{-12}, s^{-1}	3.21E+12	4.55E+12	6.02E+12
13. $Z^-[Fe(OH)_2]^+ \{M=4\} + N_2O\ (g) \leftrightarrow Z^-[Fe(OH)_2]^+(ON_2)\ \{M=4\}$	$\Delta H_{13} = -0.5$	K_{13}, bar^{-1}	9.41E−05	8.70E−05	8.42E−05
	$E_{13}^{\ddagger} = 0.0$	A_{13}, $s^{-1}\ bar^{-1}$	2.02E+08	2.81E+08	3.75E+08
		k_{13}, $s^{-1}\ bar^{-1}$	2.02E+08	2.81E+08	3.75E+08
	$E_{-13}^{\ddagger} = 2.1$	A_{-13}, s^{-1}	1.25E+13	1.46E+13	1.67E+13
		k_{-13}, s^{-1}	2.15E+12	3.23E+12	4.45E+12
14. $Z^-[OFe(OH)_2]^+ \{M=4\} + N_2O\ (g) \leftrightarrow Z^-[OFe(OH)_2]^+(ON_2)\ \{M=4\}$	$\Delta H_{14} = -5.4$	K_{14}, bar^{-1}	3.91E−04	2.01E−04	1.25E−04
	$E_{14}^{\ddagger} = 0.0$	A_{14}, $s^{-1}\ bar^{-1}$	3.06E+07	3.79E+07	4.62E+07
		k_{14}, $s^{-1}\ bar^{-1}$	3.06E+07	3.79E+07	4.62E+07
	$E_{-14}^{\ddagger} = 6.1$	A_{-14}, s^{-1}	1.25E+13	1.46E+13	1.67E+13
		k_{-14}, s^{-1}	7.82E+10	1.88E+11	3.71E+11

TABLE 1 (Continued)

reaction	$E^{\ddagger}$, ΔH^b kcal/mol	constant	*T*, K 600	700	800
Part c					
15. $Z^-[Fe]^+ \{M=6\} + N_2O$ (g) ↔ $Z^-[Fe]^+(N_2O) \{M=6\}$	$\Delta H_{15} = -13.3$	K_{15}, bar^{-1}	3.63E−02	7.25E−03	2.23E−03
	$E_{15}^{\ddagger} = 0.0$	A_{15}, s^{-1} bar^{-1}	1.16E+07	1.63E+07	2.20E+07
		k_{15}, s^{-1} bar^{-1}	2.06E+06	2.78E+06	3.66E+06
	$E_{-15}^{\ddagger} = 14.7$	A_{-15}, s^{-1}	1.25E+13	1.46E+13	1.67E+13
		k_{-15}, s^{-1}	5.68E+07	3.84E+08	1.64E+09
16. $Z^-[FeO]^+ \{M=6\} + N_2O$ (g) ↔ $Z^-[FeO]^+(N_2O) \{M=6\}$	$\Delta H_{16} = -10.1$	K_{16}, bar^{-1}	5.74E−03	1.67E−03	6.79E−04
	$E_{16}^{\ddagger} = 0.0$	A_{16}, s^{-1} bar^{-1}	4.06E+06	5.57E+06	7.38E+06
		k_{16}, s^{-1} bar^{-1}	4.06E+06	5.57E+06	7.38E+06
	$E_{-16}^{\ddagger} = 11.7$	A_{-16}, s^{-1}	1.25E+13	1.46E+13	1.67E+13
		k_{-16}, s^{-1}	7.07E+08	3.34E+09	1.09E+10
17. $Z^-[FeO_2]^+ \{M=6\} + N_2O$ (g) ↔ $Z^-[FeO_2]^+(N_2O) \{M=6\}$	$\Delta H_{17} = -2.3$	K_{17}, bar^{-1}	5.69E−06	4.25E−06	3.50E−06
	$E_{17}^{\ddagger} = 0.0$	A_{17}, s^{-1} bar^{-1}	3.05E+06	4.17E+06	5.50E+06
		k_{17}, s^{-1} bar^{-1}	3.05E+06	4.17E+06	5.50E+06
	$E_{-17}^{\ddagger} = 3.8$	A_{-17}, s^{-1}	1.25E+13	1.46E+13	1.67E+13
		k_{-17}, s^{-1}	5.36E+11	9.81E+11	1.57E+12
18. $Z^-[OFeO]^+ \{M=6\} + N_2O$ (g) ↔ $Z^-[OFeO]^+(N_2O) \{M=6\}$	$\Delta H_{18} = -3.2$	K_{18}, bar^{-1}	1.42E−05	9.53E−06	7.26E−06
	$E_{18}^{\ddagger} = 0.0$	A_{18}, s^{-1} bar^{-1}	3.57E+06	4.89E+06	6.47E+06
		k_{18}, s^{-1} bar^{-1}	3.57E+06	4.89E+06	6.47E+06
	$E_{-18}^{\ddagger} = 4.7$	A_{-18}, s^{-1}	1.25E+13	1.46E+13	1.67E+13
		k_{-18}, s^{-1}	2.52E+11	5.13E+11	8.91E+11
19. $Z^-[O_2FeO]^+ \{M=6\} + N_2O$ (g) ↔ $Z^-[O_2FeO]^+(N_2O) \{M=6\}$	$\Delta H_{19} = 1.4$	K_{19}, bar^{-1}	1.32E−06	1.53E−06	1.76E−06
	$E_{19}^{\ddagger} = 0.0$	A_{19}, s^{-1} bar^{-1}	1.41E+07	1.94E+07	2.59E+07
		k_{19}, s^{-1} bar^{-1}	1.41E+07	1.94E+07	2.59E+07
	$E_{-19}^{\ddagger} = 0.2$	A_{-19}, s^{-1}	1.25E+13	1.46E+13	1.67E+13
		k_{-19}, s^{-1}	1.06E+13	1.27E+13	1.47E+13
20. $Z^-[Fe(OH)_2]^+ \{M=6\} + N_2O$ (g) ↔ $Z^-[Fe(OH)_2]^+(N_2O) \{M=6\}$	$\Delta H_{20} = 0.4$	K_{20}, bar^{-1}	7.32E−05	7.52E−05	7.86E−05
	$E_{20}^{\ddagger} = 0.0$	A_{20}, s^{-1} bar^{-1}	3.39E+08	4.68E+08	6.23E+08
		k_{20}, s^{-1} bar^{-1}	3.39E+08	4.68E+08	6.23E+08
	$E_{-20}^{\ddagger} = 1.2$	A_{-20}, s^{-1}	1.25E+13	1.46E+13	1.67E+13
		k_{-20}, s^{-1}	4.63E+12	6.23E+12	7.92E+12
21. $Z^-[OFe(OH)_2]^+ \{M=6\} + N_2O$ (g) ↔ $Z^-[OFe(OH)_2]^+(N_2O) \{M=6\}$	$\Delta H_{21} = -0.2$	K_{21}, bar^{-1}	1.56E−04	1.50E−04	1.50E−04
	$E_{21}^{\ddagger} = 0.0$	A_{21}, s^{-1} bar^{-1}	4.76E+08	6.54E+08	8.67E+08
		k_{21}, s^{-1} bar^{-1}	4.76E+08	6.54E+08	8.67E+08
	$E_{-21}^{\ddagger} = 1.7$	A_{-21}, s^{-1}	1.25E+13	1.46E+13	1.67E+13
		k_{-21}, s^{-1}	3.05E+12	4.36E+12	5.79E+12
Part d					
22. $Z^-[Fe]^+ \{M=6\} + N_2O$ (g) ↔ $Z^-[Fe]^+(ON_2) \{M=6\}$	$\Delta H_{22} = 1.9$	K_{22}, bar^{-1}	2.10E−04	2.60E−04	3.13E−04
	$E_{22}^{\ddagger} = 0.03$	A_{22}, s^{-1} bar^{-1}	2.69E+09	3.86E+09	5.30E+09
		k_{22}, s^{-1} bar^{-1}	2.63E+09	3.79E+09	5.21E+09
	$E_{-22}^{\ddagger} = 0.0$	A_{-22}, s^{-1}	1.25E+13	1.46E+13	1.67E+13
		k_{-22}, s^{-1}	1.25E+13	1.46E+13	1.67E+13
23. $Z^-[FeO]^+ \{M=6\} + N_2O$ (g) ↔ $Z^-[FeO]^+(ON_2) \{M=6\}$	$\Delta H_{23} = -4.8$	K_{23}, bar^{-1}	9.55E−05	5.28E−05	3.48E−05
	$E_{23}^{\ddagger} = 0.0$	A_{23}, s^{-1} bar^{-1}	5.75E+06	7.95E+06	1.06E+07
		k_{23}, s^{-1} bar^{-1}	5.75E+06	7.95E+06	1.06E+07
	$E_{-23}^{\ddagger} = 6.4$	A_{-23}, s^{-1}	1.25E+13	1.46E+13	1.67E+13
		k_{-23}, s^{-1}	6.02E+10	1.51E+11	3.05E+11
24. $Z^-[FeO_2]^+ \{M=6\} + N_2O$ (g) ↔ $Z^-[FeO_2]^+(ON_2) \{M=6\}$	$\Delta H_{24} = -1.2$	K_{24}, bar^{-1}	1.73E−06	1.47E−06	1.33E−06
	$E_{24}^{\ddagger} = 0.0$	A_{24}, s^{-1} bar^{-1}	2.19E+06	3.01E+06	3.99E+06
		k_{24}, s^{-1} bar^{-1}	2.19E+06	3.01E+06	3.99E+06
	$E_{-24}^{\ddagger} = 2.7$	A_{-24}, s^{-1}	1.25E+13	1.46E+13	1.67E+13
		k_{-24}, s^{-1}	1.27E+12	2.05E+12	2.99E+12
25. $Z^-[OFeO]^+ \{M=6\} + N_2O$ (g) ↔ $Z^-[OFeO]^+(ON_2) \{M=6\}$	$\Delta H_{25} = -3.0$	K_{25}, bar^{-1}	5.35E−06	3.66E−06	2.82E−06
	$E_{25}^{\ddagger} = 0.0$	A_{25}, s^{-1} bar^{-1}	1.51E+06	2.07E+06	2.74E+06
		k_{25}, s^{-1} bar^{-1}	1.51E+06	2.07E+06	2.74E+06
	$E_{-25}^{\ddagger} = 4.5$	A_{-25}, s^{-1}	1.25E+13	1.46E+13	1.67E+13
		k_{-25}, s^{-1}	2.82E+11	5.66E+11	9.71E+11
26. $Z^-[O_2FeO]^+ \{M=6\} + N_2O$ (g) ↔ $Z^-[O_2FeO]^+(ON_2) \{M=6\}$	$\Delta H_{26} = 0.3$	K_{26}, bar^{-1}	1.32E−06	1.35E−06	1.41E−06
	$E_{26}^{\ddagger} = 0.0$	A_{26}, s^{-1} bar^{-1}	5.98E+06	8.24E+06	1.09E+07
		k_{26}, s^{-1} bar^{-1}	5.98E+06	8.24E+06	1.09E+07
	$E_{-26}^{\ddagger} = 1.2$	A_{-26}, s^{-1}	1.25E+13	1.46E+13	1.67E+13
		k_{-26}, s^{-1}	4.52E+12	6.10E+12	7.77E+12
27. $Z^-[Fe(OH)_2]^+ \{M=6\} + N_2O$ (g) ↔ $Z^-[Fe(OH)_2]^+(ON_2) \{M=6\}$	$\Delta H_{27} = 0.2$	K_{27}, bar^{-1}	8.31E−05	8.35E−05	8.59E−05
	$E_{27}^{\ddagger} = 0.0$	A_{27}, s^{-1} bar^{-1}	3.42E+08	4.70E+08	6.23E+08
		k_{27}, s^{-1} bar^{-1}	3.42E+08	4.70E+08	6.23E+08
	$E_{-27}^{\ddagger} = 1.3$	A_{-27}, s^{-1}	1.25E+13	1.46E+13	1.67E+13
		k_{-27}, s^{-1}	4.12E+12	5.63E+12	7.25E+12
28. $Z^-[OFe(OH)_2]^+ \{M=6\} + N_2O$ (g) ↔ $Z^-[OFe(OH)_2]^+(ON_2) \{M=6\}$	$\Delta H_{28} = -0.5$	K_{28}, bar^{-1}	2.95E−05	2.72E−05	2.62E−05
	$E_{28}^{\ddagger} = 0.0$	A_{28}, s^{-1} bar^{-1}	6.64E+07	9.12E+07	1.21E+08
		k_{28}, s^{-1} bar^{-1}	6.64E+07	9.12E+07	1.21E+08
	$E_{-28}^{\ddagger} = 2.0$	A_{-28}, s^{-1}	1.25E+13	1.46E+13	1.67E+13
		k_{-28}, s^{-1}	2.25E+12	3.36E+12	4.61E+12

TABLE 1 (Continued)

reaction	$E^{\ddagger}$, ΔH^b kcal/mol	constant	*T*, K 600	700	800
Part e					
29. $Z^-[Fe]^+(ON_2)$ {$M=6$} ↔ $Z^-[FeO]^+$ {$M=6$} + N_2 (g)	$\Delta H_{29} = -67.9$	K_{29}, bar	2.81E+28	8.35E+24	1.85E+22
	$E_{29}^{\ddagger} = 2.8$	A_{29}, s^{-1}	6.28E+09	6.36E+09	6.43E+09
		k_{29}, s^{-1}	6.24E+08	8.77E+08	1.14E+09
	$E_{-29}^{\ddagger} = 70.0$	A_{-29}, s^{-1} bar^{-1}	7.43E+05	7.94E+05	8.54E+05
		k_{-29}, s^{-1} bar^{-1}	2.22E−20	1.05E−16	6.14E−14
30. $Z^-[FeO]^+(ON_2)$ {$M=4$} ↔ $Z^-[FeO_2]^+$ {$M=4$} + N_2 (g)	$\Delta H_{30} = -25.7$	K_{30}, bar	2.18E+14	1.02E+13	1.00E+12
	$E_{30}^{\ddagger} = 29.0$	A_{30}, s^{-1}	3.77E+12	4.12E+12	4.43E+12
		k_{30}, s^{-1}	1.04E+02	3.67E+03	5.34E+04
	$E_{-30}^{\ddagger} = 53.7$	A_{-30}, s^{-1} bar^{-1}	1.79E+07	2.15E+07	2.55E+07
		k_{-30}, s^{-1} bar^{-1}	4.79E−13	3.60E−10	5.32E−08
31. $Z^-[FeO]^+(ON_2)$ {$M=4$} ↔ $Z^-[OFeO]^+$ {$M=4$} + N_2 (g)	$\Delta H_{31} = -17.5$	K_{31}, bar	3.27E+11	4.09E+10	8.38E+09
	$E_{31}^{\ddagger} = 27.5$	A_{31}, s^{-1}	1.00E+13	1.15E+13	1.28E+13
		k_{31}, s^{-1}	9.83E+02	3.03E+04	4.00E+05
	$E_{-31}^{\ddagger} = 43.9$	A_{-31}, s^{-1} bar^{-1}	3.11E+07	3.96E+07	4.91E+07
		k_{-31}, s^{-1} bar^{-1}	3.00E−09	7.41E−07	4.78E−05
32. $Z^-[FeO_2]^+(ON_2)$ {$M=4$} ↔ $Z^-[O_2FeO]^+$ {$M=4$} + N_2 (g)	$\Delta H_{32} = -16.8$	K_{32}, bar	2.61E+12	3.53E+11	7.72E+10
	$E_{32}^{\ddagger} = 24.0$	A_{32}, s^{-1}	8.44E+13	9.88E+13	1.12E+14
		k_{32}, s^{-1}	1.49E+05	3.10E+06	3.06E+07
	$E_{-32}^{\ddagger} = 40.3$	A_{-32}, s^{-1} bar^{-1}	2.86E+07	3.49E+07	4.19E+07
		k_{-32}, s^{-1} bar^{-1}	5.71E−08	8.78E−06	3.96E−04
33. $Z^-[OFeO]^+(ON_2)$ {$M=4$} ↔ $Z^-[O_2FeO]^+$ {$M=4$} + N_2 (g)	$\Delta H_{33} = -28.8$	K_{33}, bar	4.92E+17	1.59E+16	1.19E+15
	$E_{33}^{\ddagger} = 42.9$	A_{33}, s^{-1}	6.63E+13	7.88E+13	9.07E+13
		k_{33}, s^{-1}	1.58E−02	3.21E+00	1.74E+02
	$E_{-33}^{\ddagger} = 71.5$	A_{-33}, s^{-1} bar^{-1}	3.72E+06	4.41E+06	5.18E+06
		k_{-33}, s^{-1} bar^{-1}	3.22E−20	2.02E−16	1.47E−13
34. $Z^-[Fe(OH)_2]^+(ON_2)$ {$M=4$} ↔ $Z^-[OFe(OH)_2]^+$ {$M=4$} + N_2 (g)	$\Delta H_{34} = 5.75$	K_{34}, bar	4.93E+02	9.95E+02	1.66E+03
	$E_{34}^{\ddagger} = 54.4$	A_{34}, s^{-1}	1.92E+11	1.96E+11	1.99E+11
		k_{34}, s^{-1}	2.86E−09	1.98E−06	2.68E−04
	$E_{-34}^{\ddagger} = 48.4$	A_{-34}, s^{-1} bar^{-1}	2.60E+06	2.69E+06	2.81E+06
		k_{-34}, s^{-1} bar^{-1}	5.79E−12	1.99E−09	1.62E−07
35. $Z^-[OFe(OH)_2]^+(ON_2)$ {$M=4$} ↔ $Z^-[O_2Fe(OH)_2]^+$ {$M=4$} + N_2 (g)	$\Delta H_{35} = 30.4$	K_{35}, bar	1.15E−07	4.45E−06	6.82E−05
	$E_{35}^{\ddagger} = 52.2$	A_{35}, s^{-1}	7.61E+11	8.46E+11	9.22E+11
		k_{35}, s^{-1}	6.90E−08	4.03E−05	4.82E−03
	$E_{-35}^{\ddagger} = 21.8$	A_{-35}, s^{-1} bar^{-1}	5.29E+07	5.84E+07	6.42E+07
		k_{-35}, s^{-1} bar^{-1}	6.00E−01	9.05E+00	7.07E+01
Part f					
36. $Z^-[FeO]^+(ON_2)$ {$M=6$} ↔ $Z^-[FeO_2]^+$ {$M=6$} + N_2 (g)	$\Delta H_{36} = -20.0$	K_{36}, bar	1.78E+13	1.65E+12	2.71E+11
	$E_{36}^{\ddagger} = 30.4$	A_{36}, s^{-1}	5.40E+13	6.22E+13	6.98E+13
		k_{36}, s^{-1}	4.48E+02	1.97E+04	3.41E+05
	$E_{-36}^{\ddagger} = 50.0$	A_{-36}, s^{-1} bar^{-1}	4.19E+07	4.97E+07	5.82E+07
		k_{-36}, s^{-1} bar^{-1}	2.52E−11	1.20E−08	1.26E−06
37. $Z^-[FeO]^+(ON_2)$ {$M=6$} $Z^-[OFeO]^+$ {$M=6$} + N_2 (g)	$\Delta H_{37} = -11.8$	K_{37}, bar	6.69E+09	1.64E+09	5.61E+08
	$E_{37}^{\ddagger} = 30.7$	A_{37}, s^{-1}	1.58E+14	1.84E+14	2.09E+14
		k_{37}, s^{-1}	1.06E+03	4.87E+04	8.71E+05
	$E_{-37}^{\ddagger} = 41.9$	A_{-37}, s^{-1} bar^{-1}	2.97E+08	3.67E+08	4.43E+08
		k_{-37}, s^{-1} bar^{-1}	1.58E−07	2.97E−05	1.55E−03
38. $Z^-[FeO_2]^+(ON_2)$ {$M=6$} ↔ $Z^-[O_2FeO]^+$ {$M=6$} + N_2 (g)	$\Delta H_{38} = -12.0$	K_{38}, bar	3.84E+05	2.10E+05	1.24E+05
	$E_{38}^{\ddagger} = 20.1$	A_{38}, s^{-1}	5.91E+09	1.56E+10	3.12E+10
		k_{38}, s^{-1}	2.75E+02	8.11E+03	9.88E+04
	$E_{-38}^{\ddagger} = 31.5$	A_{-38}, s^{-1} bar^{-1}	2.12E+08	2.63E+08	3.19E+08
		k_{-38}, s^{-1} bar^{-1}	7.17E−04	3.87E−02	7.95E−01
39. $Z^-[OFeO]^+(ON_2)$ {$M=6$} ↔ $Z^-[O_2FeO]^+$ {$M=6$} + N_2 (g)	$\Delta H_{39} = -18.3$	K_{39}, bar	1.44E+13	1.63E+12	3.12E+11
	$E_{39}^{\ddagger} = 16.5$	A_{39}, s^{-1}	2.35E+14	2.81E+14	3.25E+14
		k_{39}, s^{-1}	2.27E+08	1.96E+09	1.00E+10
	$E_{-39}^{\ddagger} = 34.4$	A_{-39}, s^{-1} bar^{-1}	5.47E+07	6.75E+07	8.16E+07
		k_{-39}, s^{-1} bar^{-1}	1.57E−05	1.20E−03	3.21E−02
40. $Z^-[O_2FeO]^+(ON_2)$ {$M=6$} ↔ $Z^-[O_2FeO_2]^+$ {$M=6$} + N_2 (g)	$\Delta H_{40} = -25.5$	K_{40}, bar	5.67E+16	2.71E+15	2.73E+14
	$E_{40}^{\ddagger} = 41.1$	A_{40}, s^{-1}	4.42E+13	5.14E+13	5.81E+13
		k_{40}, s^{-1}	4.48E−02	7.22E+00	3.30E+02
	$E_{-40}^{\ddagger} = 66.9$	A_{-40}, s^{-1} bar^{-1}	1.99E+06	2.19E+06	2.42E+06
		k_{-40}, s^{-1} bar^{-1}	7.91E−19	2.66E−15	1.21E−12
41. $Z^-[Fe(OH)_2]^+(ON_2)$ {$M=6$} ↔ $Z^-[OFe(OH)_2]^+$ {$M=6$} + N_2 (g)	$\Delta H_{41} = 16.7$	K_{41}, bar	1.35E−03	1.01E−02	4.47E−02
	$E_{41}^{\ddagger} = 42.8$	A_{41}, s^{-1}	2.02E+10	2.13E+10	2.25E+10
		k_{41}, s^{-1}	5.01E−06	8.99E−04	4.44E−02
	$E_{-41}^{\ddagger} = 25.1$	A_{-41}, s^{-1} bar^{-1}	5.09E+06	6.05E+06	7.09E+06
		k_{-41}, s^{-1} bar^{-1}	3.70E−03	8.89E−02	9.93E−01
42. $Z^-[OFe(OH)_2]^+(ON_2)$ {$M=6$} ↔ $Z^-[O_2Fe(OH)_2]^+$ {$M=6$} + N_2 (g)	$\Delta H_{42} = 19.4$	K_{42}, bar	1.72E−04	1.79E−03	1.02E−02
	$E_{42}^{\ddagger} = 61.7$	A_{42}, s^{-1}	6.02E+14	7.79E+14	9.58E+14
		k_{42}, s^{-1}	1.90E−08	4.03E−05	1.28E−02
	$E_{-42}^{\ddagger} = 41.2$	A_{-42}, s^{-1} bar^{-1}	1.11E+11	1.63E+11	2.23E+11
		k_{-42}, s^{-1} bar^{-1}	1.10E−04	2.25E−02	1.25E+00

TABLE 1 (Continued)

reaction	$E^{\ddagger}$, ΔH^b kcal/mol	constant	*T*, K 600	700	800
	Part g				
43. $Z^-[Fe]^+ \{M=4\} \leftrightarrow Z^-[Fe]^+ \{M=6\}$	$\Delta H_{43} = 0.1$	K_{43}, –	1.49E+00	1.51E+00	1.53E+00
	$E_{43}^{\ddagger} = 0.3$	A_{43}, s^{-1}	1.25E+13	1.46E+13	1.67E+13
		k_{43}, s^{-1}	9.52E+12	1.15E+13	1.36E+13
	$E_{-43}^{\ddagger} = 0.3$	A_{-43}, s^{-1}	7.94E+12	9.20E+12	1.05E+13
		k_{-43}, s^{-1}	6.39E+12	7.64E+12	8.89E+12
44. $Z^-[FeO]^+ \{M=4\} \leftrightarrow Z^-[FeO]^+ \{M=6\}$	$\Delta H_{44} = -3.7$	K_{44}, –	5.47E+01	3.53E+01	2.54E+01
	$E_{44}^{\ddagger} = 2.3$	A_{44}, s^{-1}	1.25E+13	1.46E+13	1.67E+13
		k_{44}, s^{-1}	1.77E+12	2.73E+12	3.85E+12
	$E_{-44}^{\ddagger} = 5.9$	A_{-44}, s^{-1}	4.65E+12	5.47E+12	6.30E+12
		k_{-44}, s^{-1}	3.24E+10	7.74E+10	1.52E+11
45. $Z^-[FeO_2]^+ \{M=4\} \leftrightarrow Z^-[FeO_2]^+ \{M=6\}$	$\Delta H_{45} = -1.7$	K_{45}, –	4.68E+01	3.81E+01	3.26E+01
	$E_{45}^{\ddagger} = 2.9$	A_{45}, s^{-1}	1.25E+13	1.46E+13	1.67E+13
		k_{45}, s^{-1}	1.07E+12	1.77E+12	2.63E+12
	$E_{-45}^{\ddagger} = 5.0$	A_{-45}, s^{-1}	1.54E+12	1.72E+12	1.90E+12
		k_{-45}, s^{-1}	2.28E+10	4.65E+10	8.07E+10
46. $Z^-[O_2FeO]^+ \{M=4\} \leftrightarrow Z^-[O_2FeO]^+ \{M=6\}$	$\Delta H_{46} = 1.2$	K_{46}, –	1.15E−01	1.32E−01	1.47E−01
	$E_{46}^{\ddagger} = 21.6$	A_{46}, s^{-1}	1.25E+13	1.46E+13	1.67E+13
		k_{46}, s^{-1}	1.63E+05	2.54E+06	2.03E+07
	$E_{-46}^{\ddagger} = 20.2$	A_{-46}, s^{-1}	3.25E+13	3.91E+13	4.59E+13
		k_{-46}, s^{-1}	1.41E+06	1.92E+07	1.38E+08
47. $Z^-[FeO_2]^+ \{M=4\} \leftrightarrow Z^-[Fe]^+ \{M=4\} + O_2$ (g)	$\Delta H_{47} = 50.3$	K_{47}, bar	2.09E−11	8.86E−09	8.05E−07
	$E_{47}^{\ddagger} = 50.9$	A_{47}, s^{-1}	1.25E+13	1.46E+13	1.67E+13
		k_{47}, s^{-1}	3.53E−06	1.84E−03	2.04E−01
	$E_{-47}^{\ddagger} = 0.0$	A_{-47}, s^{-1} bar^{-1}	1.69E+05	2.08E+05	2.54E+05
		k_{-47}, s^{-1} bar^{-1}	1.69E+05	2.08E+05	2.54E+05
48. $Z^-[O_2FeO]^+ \{M=4\} \leftrightarrow Z^-[FeO]^+ \{M=4\} + O_2$ (g)	$\Delta H_{48} = 4.2$	K_{48}, bar	2.85E+05	4.80E+05	6.92E+05
	$E_{48}^{\ddagger} = 21.6$	A_{48}, s^{-1}	1.25E+13	1.46E+13	1.67E+13
		k_{48}, s^{-1}	1.63E+05	2.54E+06	2.03E+07
	$E_{-48}^{\ddagger} = 16.7$	A_{-48}, s^{-1} bar^{-1}	7.14E+05	8.91E+05	1.10E+06
		k_{-48}, s^{-1} bar^{-1}	5.70E−01	5.29E+00	2.93E+01
49. $Z^-[O_2Fe(OH)_2]^+ \{M=4\} \leftrightarrow Z^-[Fe(OH)_2]^+ \{M=4\} + O_2$ (g)	$\Delta H_{49} = -68.8$	K_{49}, bar	3.20E+33	8.56E+29	1.74E+27
	$E_{49}^{\ddagger} = 13.1$	A_{49}, s^{-1}	1.72E+13	1.83E+13	1.92E+13
		k_{49}, s^{-1}	2.94E+08	1.50E+09	5.10E+09
	$E_{-49}^{\ddagger} = 81.5$	A_{-49}, s^{-1} bar^{-1}	4.70E+04	5.11E+04	5.60E+04
		k_{-49}, s^{-1} bar^{-1}	9.18E−26	1.75E−21	2.93E−18
	Part h				
50. $Z^-[FeO_2]^+ \{M=6\} \leftrightarrow Z^-[Fe]^+ \{M=4\} + O_2$ (g)	$\Delta H_{50} = 52.0$	K_{50}, bar	4.47E−13	2.33E−10	2.47E−08
	$E_{50}^{\ddagger} = 53.0$	A_{50}, s^{-1}	1.25E+13	1.46E+13	1.67E+13
		k_{50}, s^{-1}	6.14E−07	4.11E−04	5.50E−02
	$E_{-50}^{\ddagger} = 0.0$	A_{-50}, s^{-1} bar^{-1}	1.37E+06	1.76E+06	2.23E+06
		k_{-50}, s^{-1} bar^{-1}	1.37E+06	1.76E+06	2.23E+06
51. $Z^-[FeO_2]^+ \{M=6\} \leftrightarrow Z^-[Fe]^+ \{M=6\} + O_2$ (g)	$\Delta H_{51} = 52.1$	K_{51}, bar	6.66E−13	3.52E−10	3.77E−08
	$E_{51}^{\ddagger} = 54.2$	A_{51}, s^{-1}	1.25E+13	1.46E+13	1.67E+13
		k_{51}, s^{-1}	2.28E−07	1.76E−04	2.62E−02
	$E_{-51}^{\ddagger} = 1.1$	A_{-51}, s^{-1} bar^{-1}	8.73E+05	1.11E+06	1.40E+06
		k_{-51}, s^{-1} bar^{-1}	3.43E+05	5.00E+05	6.94E+05
52. $Z^-[O_2FeO]^+ \{M=6\} \leftrightarrow Z^-[FeO]^+ \{M=4\} + O_2$ (g)	$\Delta H_{52} = 3.0$	K_{52}, bar	2.48E+06	3.63E+06	4.72E+06
	$E_{52}^{\ddagger} = 6.9$	A_{52}, s^{-1}	1.25E+14	1.39E+14	1.51E+14
		k_{52}, s^{-1}	3.69E+11	9.43E+11	1.91E+12
	$E_{-52}^{\ddagger} = 3.5$	A_{-52}, s^{-1} bar^{-1}	2.76E+06	3.17E+06	3.61E+06
		k_{-52}, s^{-1} bar^{-1}	1.49E+05	2.60E+05	4.04E+05
53. $Z^-[O_2FeO]^+ \{M=6\} \leftrightarrow Z^-[FeO]^+ \{M=6\} + O_2$ (g)	$\Delta H_{53} = -0.6$	K_{53}, bar	1.36E+08	1.28E+08	1.20E+08
	$E_{53}^{\ddagger} = 8.0$	A_{53}, s^{-1}	1.25E+13	1.46E+13	1.67E+13
		k_{53}, s^{-1}	1.56E+10	4.72E+10	1.11E+11
	$E_{-53}^{\ddagger} = 8.1$	A_{-53}, s^{-1} bar^{-1}	1.02E+05	1.24E+05	1.51E+05
		k_{-53}, s^{-1} bar^{-1}	1.15E+02	3.68E+02	9.23E+02
54. $Z^-[O_2FeO_2]^+ \{M=6\} \leftrightarrow Z^-[FeO_2]^+ \{M=4\} + O_2$ (g)	$\Delta H_{54} = 1.5$	K_{54}, bar	6.55E+04	8.00E+04	9.02E+04
	$E_{54}^{\ddagger} = 11.4$	A_{54}, s^{-1}	2.10E+13	2.24E+13	2.35E+13
		k_{54}, s^{-1}	1.52E+09	6.33E+09	1.84E+10
	$E_{-54}^{\ddagger} = 8.3$	A_{-54}, s^{-1} bar^{-1}	2.51E+07	3.16E+07	3.85E+07
		k_{-54}, s^{-1} bar^{-1}	2.32E+04	7.91E+04	2.04E+05
55. $Z^-[O_2FeO_2]^+ \{M=6\} \leftrightarrow Z^-[FeO_2]^+ \{M=6\} + O_2$ (g)	$\Delta H_{55} = -0.2$	K_{55}, bar	3.07E+06	3.04E+06	2.94E+06
	$E_{55}^{\ddagger} = 5.8$	A_{55}, s^{-1}	1.25E+13	1.46E+13	1.67E+13
		k_{55}, s^{-1}	9.30E+10	2.18E+11	4.22E+11
	$E_{-55}^{\ddagger} = 4.9$	A_{-55}, s^{-1} bar^{-1}	1.84E+06	2.42E+06	3.11E+06
		k_{-55}, s^{-1} bar^{-1}	3.03E+04	7.18E+04	1.43E+05
56. $Z^-[O_2Fe(OH)_2]^+ \{M=6\} \leftrightarrow Z^-[Fe(OH)_2]^+ \{M=4\} + O_2$ (g)	$\Delta H_{56} = -60.2$	K_{56}, bar	3.99E+30	2.97E+27	1.31E+25
	$E_{56}^{\ddagger} = 16.0$	A_{56}, s^{-1}	3.48E+13	3.89E+13	4.23E+13
		k_{56}, s^{-1}	5.00E+07	3.82E+08	1.76E+09
	$E_{-56}^{\ddagger} = 76.2$	A_{-56}, s^{-1} bar^{-1}	7.62E+04	8.37E+04	9.25E+04
		k_{-56}, s^{-1} bar^{-1}	1.26E−23	1.28E−19	1.34E−16

TABLE 1 (Continued)

reaction	E‡, ΔH[b] kcal/mol	constant	T, K 600	700	800
	Part i				
57. $Z^-[O_2Fe(OH)_2]^+$ {$M=6$} ↔ $Z^-[Fe(OH)_2]^+$ {$M=6$} + O_2 (g)	$\Delta H_{57} = -74.3$	K_{57}, bar	1.17E+37	1.61E+33	2.01E+30
	$E_{57}^{\ddagger} = 15.8$	A_{57}, s^{-1}	1.25E+13	1.46E+13	1.67E+13
		k_{57}, s^{-1}	2.12E+07	1.65E+08	7.83E+08
	$E_{-57}^{\ddagger} = 90.9$	A_{-57}, s^{-1} bar^{-1}	2.52E+03	2.62E+03	2.81E+03
		k_{-57}, s^{-1} bar^{-1}	1.81E−30	1.02E−25	3.90E−22
58. $Z^-[FeO_2]^+$ {$M=4$} ↔ $Z^-[OFeO]^+$ {$M=4$}	$\Delta H_{58} = 8.2$	K_{58}, −	1.50E−03	4.01E−03	8.35E−03
	$E_{58}^{\ddagger} = 30.5$	A_{58}, s^{-1}	1.26E+14	1.40E+14	1.52E+14
		k_{58}, s^{-1}	9.60E+02	4.13E+04	6.97E+05
	$E_{-58}^{\ddagger} = 22.3$	A_{-58}, s^{-1}	8.24E+13	9.23E+13	1.01E+14
		k_{-58}, s^{-1}	6.38E+05	1.03E+07	8.35E+07
59. $Z^-[FeO_2]^+$ {$M=6$} ↔ $Z^-[OFeO]^+$ {$M=6$}	$\Delta H_{59} = 8.1$	K_{59}, −	3.77E−04	9.96E−04	2.07E−03
	$E_{59}^{\ddagger} = 22.5$	A_{59}, s^{-1}	7.68E+12	8.11E+12	8.46E+12
		k_{59}, s^{-1}	4.91E+04	7.68E+05	6.05E+06
	$E_{-59}^{\ddagger} = 14.1$	A_{-59}, s^{-1}	1.86E+13	2.02E+13	2.15E+13
		k_{-59}, s^{-1}	1.30E+08	7.71E+08	2.93E+09
60. $Z^-[FeO]^+$ {$M=4$} + H_2O (g) ↔ $Z^-[FeO]^+(OH_2)$ {$M=4$}	$\Delta H_{60} = -8.8$	K_{60}, bar^{-1}	1.53E−03	4.80E−04	2.08E−04
	$E_{60}^{\ddagger} = 0.0$	A_{60}, s^{-1} bar^{-1}	2.75E+06	3.56E+06	4.54E+06
		k_{60}, s^{-1} bar^{-1}	2.75E+06	3.56E+06	4.54E+06
	$E_{-60}^{\ddagger} = 10.5$	A_{-60}, s^{-1}	1.25E+13	1.46E+13	1.67E+13
		k_{-60}, s^{-1}	1.79E+09	7.41E+09	2.19E+10
61. $Z^-[FeO]^+$ {$M=6$} + H_2O (g) ↔ $Z^-[FeO]^+(OH_2)$ {$M=6$}	$\Delta H_{61} = -15.6$	K_{61}, bar^{-1}	2.58E−01	3.56E−02	8.32E−03
	$E_{61}^{\ddagger} = 0.0$	A_{61}, s^{-1} bar^{-1}	1.58E+06	2.03E+06	2.57E+06
		k_{61}, s^{-1} bar^{-1}	1.58E+06	2.03E+06	2.57E+06
	$E_{-61}^{\ddagger} = 17.3$	A_{-61}, s^{-1}	1.25E+13	1.46E+13	1.67E+13
		k_{-61}, s^{-1}	6.14E+06	5.71E+07	3.09E+08
62. $Z^-[FeO]^+(OH_2)$ {$M=4$} ↔ $Z^-[Fe(OH)_2]^+$ {$M=4$}	$\Delta H_{62} = -23.5$	K_{62}, −	5.74E+06	3.42E+05	4.14E+04
	$E_{62}^{\ddagger} = 1.9$	A_{62}, s^{-1}	1.47E+11	1.30E+11	1.19E+11
		k_{62}, s^{-1}	3.00E+10	3.34E+10	3.62E+10
	$E_{-62}^{\ddagger} = 24.6$	A_{-62}, s^{-1}	4.89E+12	4.77E+12	4.67E+12
		k_{-62}, s^{-1}	5.23E+03	9.75E+04	8.74E+05
63. $Z^-[FeO]^+(OH_2)$ {$M=6$} ↔ $Z^-[Fe(OH)_2]^+$ {$M=6$}	$\Delta H_{63} = -27.1$	K_{63}, −	1.83E+09	7.10E+07	6.26E+06
	$E_{63}^{\ddagger} = 9.2$	A_{63}, s^{-1}	2.28E+12	2.18E+12	2.13E+12
		k_{63}, s^{-1}	1.03E+09	2.97E+09	6.60E+09
	$E_{-63}^{\ddagger} = 36.4$	A_{-63}, s^{-1}	1.08E+13	1.02E+13	9.69E+12
		k_{-63}, s^{-1}	5.63E−01	4.18E+01	1.05E+03

[a] (a) N_2O adsorption from the N end, $M_S = 4$. (b) N_2O adsorption from the O end, $M_S = 4$. (c) N_2O adsorption from the N end, $M_S = 6$. (d) N_2O adsorption from the O end, $M_S = 6$. (e) N_2O dissociation, $M_S = 4$. (f) N_2O dissociation, $M_S = 6$. (g)−(i) O_2 desorption and various other reactions. ‡Calculated activation energy including zero-point energy correction. [b] Calculated enthalpy averaged over 600−800 K.

TABLE 2: Norm of the Gradient Difference at the Point of Spin Surface Crossing and Thermally Averaged Landau−Zener Transition Probabilities at Temperatures of 600, 700, and 800 K[a]

reaction[b]	|grad(E_1) − grad(E_2)| (kJ/mol/Å)	T, K P_{LZ} (H_{12} = 395 J/mol) 600	700	800	P_{LZ} (H_{12} = 825 J/mol) 600	700	800
43. $Z^-[Fe]^+$ {$M=4$} ↔ $Z^-[Fe]^+$ {$M=6$}	113	0.096	0.090	0.086	0.270	0.257	0.246
44. $Z^-[FeO]^+$ {$M=4$} ↔ $Z^-[FeO]^+$ {$M=6$}	37	0.185	0.176	0.168	0.462	0.443	0.427
45. $Z^-[FeO_2]^+$ {$M=4$} ↔ $Z^-[FeO_2]^+$ {$M=6$}	264	0.048	0.045	0.043	0.148	0.140	0.133
46. $Z^-[O_2FeO]^+$ {$M=4$} ↔ $Z^-[O_2FeO]^+$ {$M=6$}	405	0.033	0.031	0.029	0.105	0.099	0.094
47. $Z^-[FeO_2]^+$ {$M=4$} ↔ $Z^-[Fe]^+$ {$M=4$} + O_2 (g)	264	0.048	0.045	0.043	0.148	0.140	0.133
48. $Z^-[O_2FeO]^+$ {$M=4$} ↔ $Z^-[FeO]^+$ {$M=4$} + O_2 (g)	405	0.033	0.031	0.029	0.105	0.099	0.094
49. $Z^-[O_2Fe(OH)_2]^+$ {$M=4$} ↔ $Z^-[Fe(OH)_2]^+$ {$M=4$} + O_2 (g)	102	0.089	0.084	0.080	0.254	0.242	0.231
51. $Z^-[FeO_2]^+$ {$M=6$} ↔ $Z^-[Fe]^+$ {$M=6$} + O_2 (g)	113	0.095	0.090	0.085	0.269	0.256	0.245
53. $Z^-[O_2FeO]^+$ {$M=6$} ↔ $Z^-[FeO]^+$ {$M=6$} + O_2 (g)	366	0.035	0.033	0.031	0.111	0.105	0.100
55. $Z^-[O_2FeO_2]^+$ {$M=6$} ↔ $Z^-[FeO_2]^+$ {$M=6$} + O_2 (g)	173	0.068	0.064	0.061	0.201	0.190	0.182
57. $Z^-[O_2Fe(OH)_2]^+$ {$M=6$} ↔ $Z^-[Fe(OH)_2]^+$ {$M=6$} + O_2 (g)	512	0.029	0.027	0.025	0.092	0.086	0.082

[a] Landau−Zener probabilities are calculated for a spin−orbit coupling energy of H_{12} = 395 and 825 J/mol. [b] Reaction numbers are the same as in Table 1.

corresponding Fe−O bond distances are 1.81 Å ($M_S = 4$) or 1.95 Å ($M_S = 6$). Spectroscopic observations made on Fe−ZSM-5 confirm the presence of a stable form of diatomic oxygen associated with Fe. Based on ESR studies of Fe−ZSM-5, Chen et al.[66] suggested the presence of superoxide ions, O_2^-, at 77 K. On the other hand, Gao et al.[67] have reported evidence for peroxide, O_2^{2-}, species using UV−Raman spectroscopy. The calculated vibrational modes associated with O_2 in $Z^-[FeO_2]^+$ are 969 and 1015 cm^{-1} on the quartet PES and 1092 and 1103 cm^{-1} on the sextet PES. Based on the work of Che and Tench,[68] the O−O bond length and the vibrational frequency of $Z^-[FeO_2]^+$ on the sextet PES suggest a superoxide species, whereas the longer bond length and lower O−O frequency stretches on the quartet PES suggest a species somewhere between a peroxide and a superoxide anion.

Oxygen can desorb from $Z^-[FeO_2]^+$. The ground state of the oxygen molecule is a triplet $^3\Sigma_g^-$ state with two unpaired electrons. As a result, the O_2 desorption process is accompanied by a change in the spin of the zeolite cluster. If both reactant and product states are on the sextet PES, the barrier for a spin-

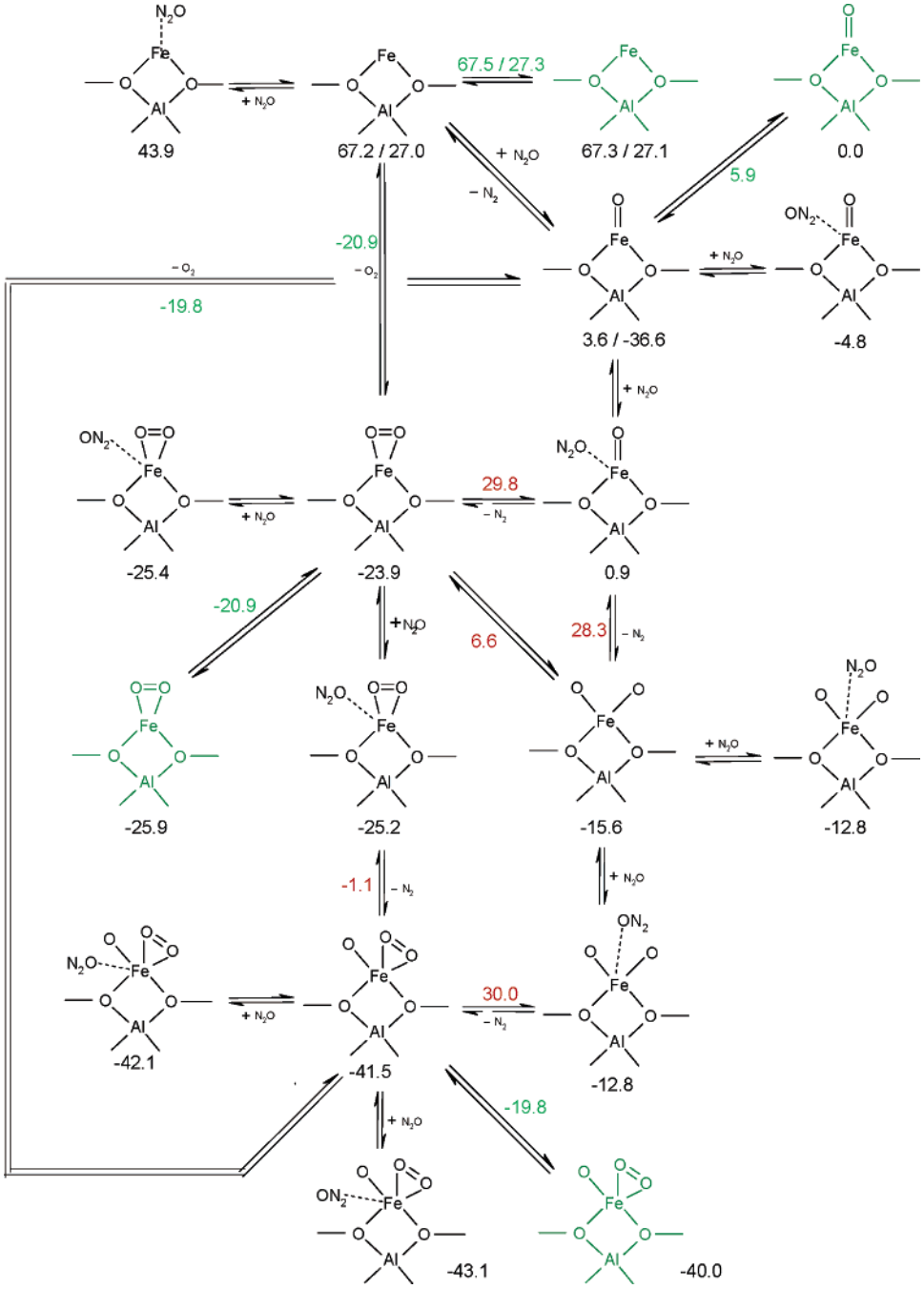

Figure 2. Reaction network of the N_2O dissociation on mononuclear iron oxo species. All energies are zero-point corrected, in kcal/mol and with reference to $Z^-[FeO]^+$ $\{M_S = 6\}$ with the appropriate amounts of N_2O, O_2, N_2, H_2O. Energies of potential energy minima are in black. Energies of transition states are in red. Energies of minima on the seam of two PES ($M_S = 4$ and $M_S = 6$) are in green. Structures in black are on the PES with $M_S = 4$. Structures in green are on the PES with $M_S = 6$.

change is calculated to be 54.1 kcal/mol (sextet/octet PES). In case the reactant is on the sextet PES and the product is on the quartet PES, there is no spin change and the energy barrier can be calculated as the energy difference between the desorbed O_2 state minus the adsorbed O_2 state, 52.9 kcal/mol (no transition state was found). If the reactant and product states are on the quartet PES, the calculated spin−surface crossing energy (quartet/sextet PES) is lower than the product-state energy, so that the effective barrier can again be calculated as the energy difference of the product and the reactant state, 50.9 kcal/mol. To conclude, the O_2 desorption barrier is larger than 50 kcal/mol. Therefore, regeneration of an active $Z^-[Fe]^+$ site is unlikely to happen under reaction conditions, and a $Z^-[Fe]^+$ site should not be considered as the active site for the nitrous oxide decomposition on Fe−ZSM-5.

Catalytic Cycle on $Z^-[FeO]^+$. As shown in the last section, $Z^-[FeO]^+$ sites are catalytically active. Parts of the catalytic cycle on $Z^-[FeO]^+$ were discussed above and will not be repeated. As noted above, one reaction pathway for the N_2O dissociation leads to $Z^-[FeO_2]^+$, whereas another leads to dioxo $Z^-[OFeO]^+$ species. The transition state for the reaction of $Z^-[FeO]^+(ON_2)$ to form $Z^-[OFeO]^+$ and N_2 is characterized by a bending of the N_2O molecule from 180° in the adsorbed state to 140.5° ($M_S = 4$) or 143.6° ($M_S = 6$) in the transition state, whereas the length of the N′−O″ bond of the N_2O molecule increases from 1.20 to 1.44 Å ($M_S = 4$) or 1.54 Å

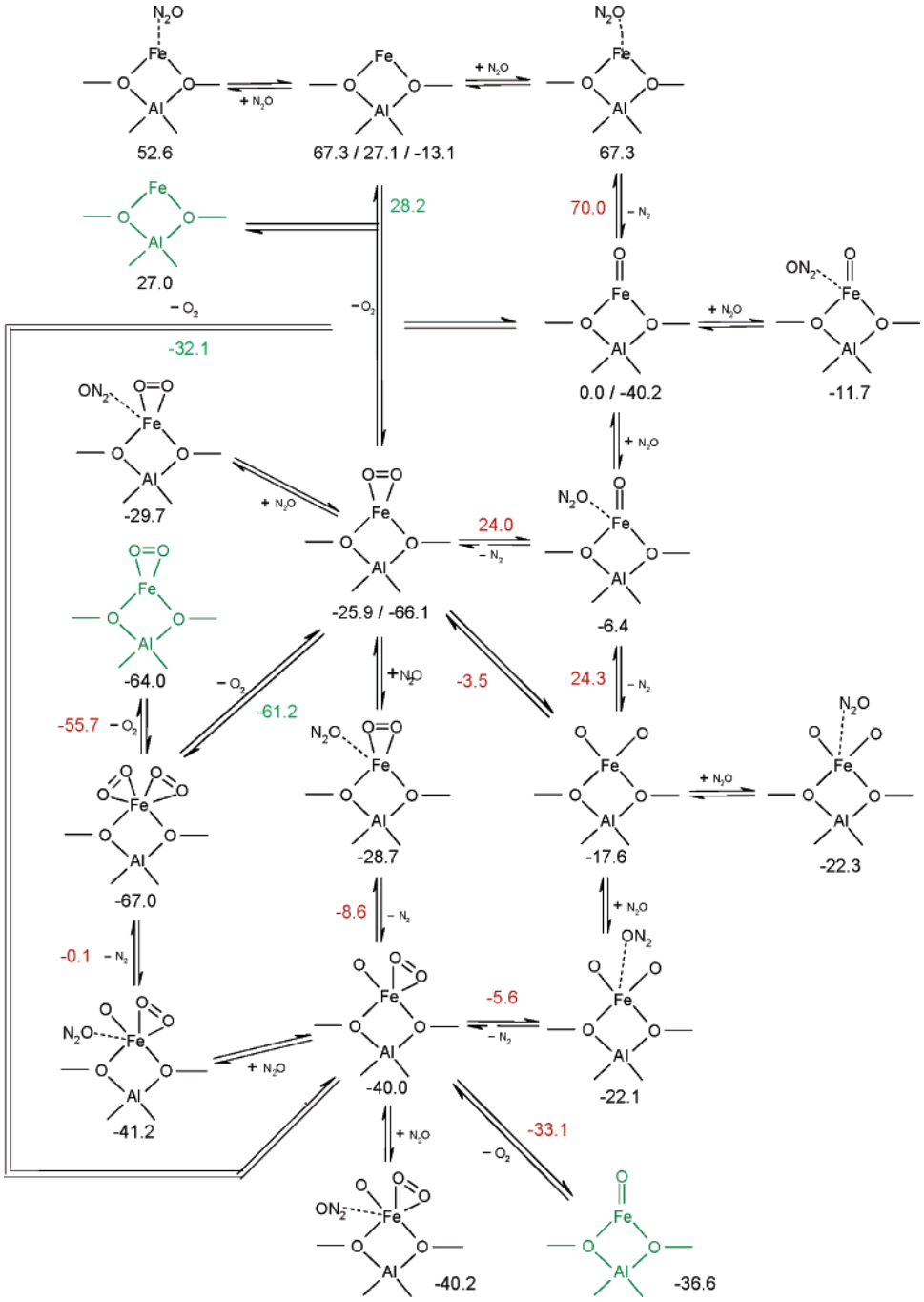

Figure 3. Reaction network of the N_2O dissociation on mononuclear iron oxo species. All energies are zero-point corrected, in kcal/mol and with reference to $Z^-[FeO]^+$ $\{M_S = 6\}$ with the appropriate amounts of N_2O, O_2, N_2, and H_2O. Energies of potential energy minima are in black. Energies of transition states are in red. Energies of minima on the seam of two PES ($M_S = 6$ and 8) are in green. Structures in black are on the PES with $M_S = 6$. Structures in green are on the PES with $M_S = 4$.

($M_S = 6$). The activation barrier for the decomposition is $E^{\ddagger}$-($M_S = 4$) = 27.5 kcal/mol or $E^{\ddagger}(M_S = 6)$ = 30.7 kcal/mol. The imaginary frequency associated with the transition state mode is 810*i* cm^{-1} ($M_S = 4$) or 892*i* cm^{-1} ($M_S = 6$). Both the transition state structures and the energetics are very similar for the reaction pathways leading to $Z^-[FeO_2]^+$ and $Z^-[OFeO]^+$.

The zero-point corrected energy of $Z^-[OFeO]^+$ on the quartet PES is approximately 2 kcal/mol higher than on the sextet PES. The surface O atoms are located 1.59 Å ($M_S = 4$) or 1.68 Å ($M_S = 6$) from the Fe atom. The O−O bond length is 2.71 Å ($M_S = 4$) or 2.32 Å ($M_S = 6$). There is no chemical bond between the two oxygen atoms. The surface oxygen atoms are much closer to the iron atom in the $Z^-[OFeO]^+$ structure than in the $Z^-[FeO_2]^+$ structure and, therefore, much more similar to $Z^-[FeO]^+$, for which the Fe−O bond length is 1.68 Å ($M_S = 4$) or 1.66 Å ($M_S = 6$). The calculated vibrational modes associated with the Fe−O stretch in $Z^-[OFeO]^+$ are 955 and 1012 cm^{-1} on the quartet PES and 643 and 868 cm^{-1} on the sextet PES. Figures 2 and 3 illustrate that the $Z^-[OFeO]^+$ species is 8.3 kcal/mol higher in energy than the $Z^-[FeO_2]^+$ species. A reaction pathway connecting $Z^-[OFeO]^+$ and $Z^-[FeO_2]^+$ was found. The activation energy for this reaction is $E^{\ddagger}(M_S = 4)$ = 22.2 kcal/mol or $E^{\ddagger}(M_S = 6)$ = 14.2 kcal/mol (starting from $Z^-[OFeO]^+$). The imaginary frequency associated with the

transition state mode is 702*i* cm^{-1} ($M_S = 4$) or 636*i* cm^{-1} ($M_S = 6$). Both $Z^-[OFeO]^+$ and $Z^-[FeO_2]^+$, should be present under reaction conditions with $Z^-[FeO_2]^+$ as the dominant species.

Both $Z^-[OFeO]^+$ and $Z^-[FeO_2]^+$ sites are catalytically active for the N_2O dissociation. N_2O adsorbs through the N end with an enthalpy of adsorption of $\Delta H_{ads}(M_S = 4) = 4.5$ kcal/mol or $\Delta H_{ads}(M_S = 6) = -3.2$ kcal/mol on $Z^-[OFeO]^+$ and with an enthalpy of adsorption of $\Delta H_{ads}(M_S = 4) = 0.3$ kcal/mol or $\Delta H_{ads}(M_S = 6) = -2.3$ kcal/mol on $Z^-[FeO_2]^+$. N_2O adsorption through the O end is as weak as through the N end: $\Delta H_{ads}(M_S = 4) = 4.5$ kcal/mol or $\Delta H_{ads}(M_S = 6) = -3.0$ kcal/mol on $Z^-[OFeO]^+$ and $\Delta H_{ads}(M_S = 4) = 0.7$ kcal/mol or $\Delta H_{ads}(M_S = 6) = -1.2$ kcal/mol on $Z^-[FeO_2]^+$. Taking into account the loss of entropy associated with the adsorption process, it follows that N_2O does not adsorb on the quartet PES and only weakly on the sextet PES.

One reaction pathway was found for N_2O dissociation from $Z^-[OFeO]^+(ON_2)$ and one for $Z^-[FeO_2]^+(ON_2)$, yielding $Z^-[O_2FeO]^+$. The transition state for the reaction leading from $Z^-[OFeO]^+(ON_2)$ to $Z^-[O_2FeO]^+$ is characterized by a bending of the N_2O molecule from 180° in the adsorbed state to 149.7° ($M_S = 4$) or 139.7° ($M_S = 6$) in the transition state. In addition, the N′−O″ bond length of the N_2O molecule increases from 1.20 to 1.68 Å ($M_S = 4$) or 1.42 Å ($M_S = 6$) in the transition state. The activation barrier for the decomposition is $E^‡(M_S = 4) = 42.9$ kcal/mol and $E^‡(M_S = 6) = 16.5$ kcal/mol. The imaginary frequency associated with the transition state mode is 790*i* cm^{-1} ($M_S = 4$) and 716*i* cm^{-1} ($M_S = 6$). From the activation barriers, it follows that the quartet PES is nonreactive, whereas the sextet PES is very reactive. From the heats of reaction, $\Delta H_R(M_S = 4) = -28.8$ kcal/mol or $\Delta H_R(M_S = 6) = -18.3$ kcal/mol, we can conclude that the reverse reaction is very slow and that decomposition is essentially irreversible.

The transition state for the reaction leading from $Z^-[FeO_2]^+(ON_2)$ to $Z^-[O_2FeO]^+$ is characterized by bending of the N_2O molecule from 180° in the adsorbed state to 140.8° ($M_S = 4$) or 139.9° ($M_S = 6$) in the transition state. In addition, the N′−O″ bond length of the N_2O molecule is increased from 1.20 to 1.44 Å ($M_S = 4$) or 1.42 Å ($M_S = 6$) in the transition state. The activation barrier for decomposition is $E^‡(M_S = 4) = 24.0$ kcal/mol or $E^‡(M_S = 6) = 20.1$ kcal/mol. The imaginary frequency associated with the transition-state mode is 732*i* cm^{-1} ($M_S = 4$) and 717*i* cm^{-1} ($M_S = 6$). Taking into account the enthalpy of reaction, $\Delta H_R(M_S = 4) = -16.8$ kcal/mol or $\Delta H_R(M_S = 6) = -12.0$ kcal/mol and transition-state energy, we conclude that the reverse reaction is slow and that decomposition is again essentially irreversible. It is important to note that the activation barrier with respect to the gas phase for N_2O decomposition on $Z^-[FeO_2]^+$ and on $Z^-[OFeO]^+$, 17.3 or 12 kcal/mol (both $M_S = 6$), is lower than the activation barrier for N_2O decomposition on $Z^-[FeO]^+$, 24.0 or 24.3 kcal/mol (both $M_S = 6$). This relationship is in opposition to conclusions drawn from experimental studies[11,36,37] and calculations reported Ryder et al.[35]

$Z^-[O_2FeO]^+$ consists of a superoxide O_2^- anion and an O^- or O^{2-} anion on top of an Fe^{2+} or Fe^{3+} cation. The O−O bond length of the superoxide O_2^- anion is 1.29 Å ($M_S = 4$) or 1.31 Å ($M_S = 6$). The Fe−O bond distance of the superoxide anion to the iron cation is 1.89 and 2.20 Å on the quartet PES and 1.91 and 2.06 Å on the sextet PES. Based on the O−O bond distance and the associated vibrational frequency, 1227 cm^{-1} ($M_S = 4$) or 1191 cm^{-1} ($M_S = 6$), the diatomic oxygen can be best described as a superoxide anion. The third O anion bonded to the iron cation has an Fe−O distance of 1.63 Å ($M_S = 4$) or 1.62 Å ($M_S = 6$) and a vibrational mode associated with Fe−O stretches of 913 cm^{-1} ($M_S = 4$) or 923 cm^{-1} ($M_S = 6$). It is interesting to note that for $Z^-[O_2FeO]^+$ the quartet PES is again preferred to the sextet PES by 1.5 kcal/mol.

Oxygen can desorb from $Z^-[O_2FeO]^+$. As mentioned above, the ground state of the oxygen molecule is a triplet $^3\Sigma_g^-$ state with two unpaired electrons so that O_2 desorption is accompanied by a spin change of the zeolite cluster. If the cluster representations of both reactant and product states lie on the sextet PES, the spin-change barrier is calculated to be 8.0 kcal/mol (sextet/octet PES) for the desorption reaction. By contrast, if the reactant state is on the sextet PES and the product state is on the quartet PES, no spin change occurs, and the transition state for the O_2 desorption can be determined. In this case, the activation barrier is $E^‡ = 6.9$ kcal/mol. The imaginary frequency associated with the transition state mode is 83*i* cm^{-1} ($M_S = 6$). Finally, for the case where the reactant and product states are on the quartet PES, the calculated spin−surface crossing barrier (quartet/sextet PES) is 21.6 kcal/mol. It is important to note that the enthalpy of O_2 desorption is very small: $\Delta H_R(M_S = 4) = 4.2$ kcal/mol, $\Delta H_R(M_S = 6) = -0.6$ kcal/mol, $\Delta H_R(M_S = 6/4) = 3.0$ kcal/mol. Therefore, O_2 desorption $Z^-[O_2FeO]^+$ from the more reactive sextet PES should be very fast. The low enthalpy of desorption is consistent with the absence of O_2 inhibition on the rate of N_2O decomposition on Fe−ZSM-5.[1,2,69,70] The adsorption process is entropically very unfavorable, so that a significant enthalpy of adsorption is required to poison $Z^-[FeO]^+$sites by O_2. The fast O_2 desorption process on the other hand is a contradiction to experimental results from Wood et al.[36] and Bulushev et al.,[37] who claim that the desorption process is the rate-limiting step in the N_2O decomposition cycle.

Catalytic Cycle on $Z^-[FeO_2]^+$. A third possible starting structure for the catalytic cycle on iron oxo sites is $Z^-[FeO_2]^+$. Since the N_2O decomposition on $Z^-[FeO_2]^+$ to produce $Z^-[O_2FeO]^+$ was examined in the preceding section, this reaction will not be discussed further here. N_2O adsorbs on $Z^-[O_2FeO]^+$ through the N end with an enthalpy of adsorption of $\Delta H_{ads}(M_S = 4) = 0.7$ kcal/mol or $\Delta H_{ads}(M_S = 6) = 1.4$ kcal/mol. N_2O adsorbs somewhat more strongly through its O end, $\Delta H_{ads}(M_S = 4) = -0.2$ kcal/mol or $\Delta H_{ads}(M_S = 6) = 0.3$ kcal/mol. However, hardly any N_2O would be expected to adsorb on $Z^-[O_2FeO]^+$ sites under reaction conditions. No reaction pathway was found for N_2O decomposition on $Z^-[O_2FeO]^+$ on the quartet PES but only on the sextet PES. The transition state for the decomposition of $Z^-[O_2FeO]^+(ON_2)$ to form $Z^-[O_2FeO_2]^+$ on the sextet PES is characterized by a bending of the N_2O molecule from 180° in the adsorbed state to 137.0° ($M_S = 6$) in the transition state and an increase in the N′−O″ bond length from 1.20 to 1.35 Å. In addition, the oxygen atom of N_2O forms a bond with the single O atom attached to Fe. The length of this O−O bond is 1.58 Å. The activation barrier for N_2O decomposition is $E^‡(M_S = 6) = 41.1$ kcal/mol and the imaginary frequency associated with the transition-state mode is 728*i* cm^{-1}. The enthalpy of reaction for this process is $\Delta H_R(M_S = 6) = -25.5$ kcal/mol. The surface oxygen atoms in $Z^-[O_2FeO_2]^+$ sites are grouped into two adsorbed superoxide anions. The surface O atoms are 2.02−2.05 Å apart from the Fe^{3+} cation. The O−O bond length of the superoxide ions is 1.31−1.32 Å. The vibrational modes associated with O−O stretches are 1170 and 1206 cm^{-1}.

Oxygen can desorb from $Z^-[O_2FeO_2]^+$. When the reactant and product states lie on the sextet PES, the spin-change barrier is calculated to be 5.8 kcal/mol (sextet/octet PES) and the enthalpy of desorption is $\Delta H_R(M_S = 6) = -0.2$ kcal/mol. For the case where the reactant is on the sextet PES and the product

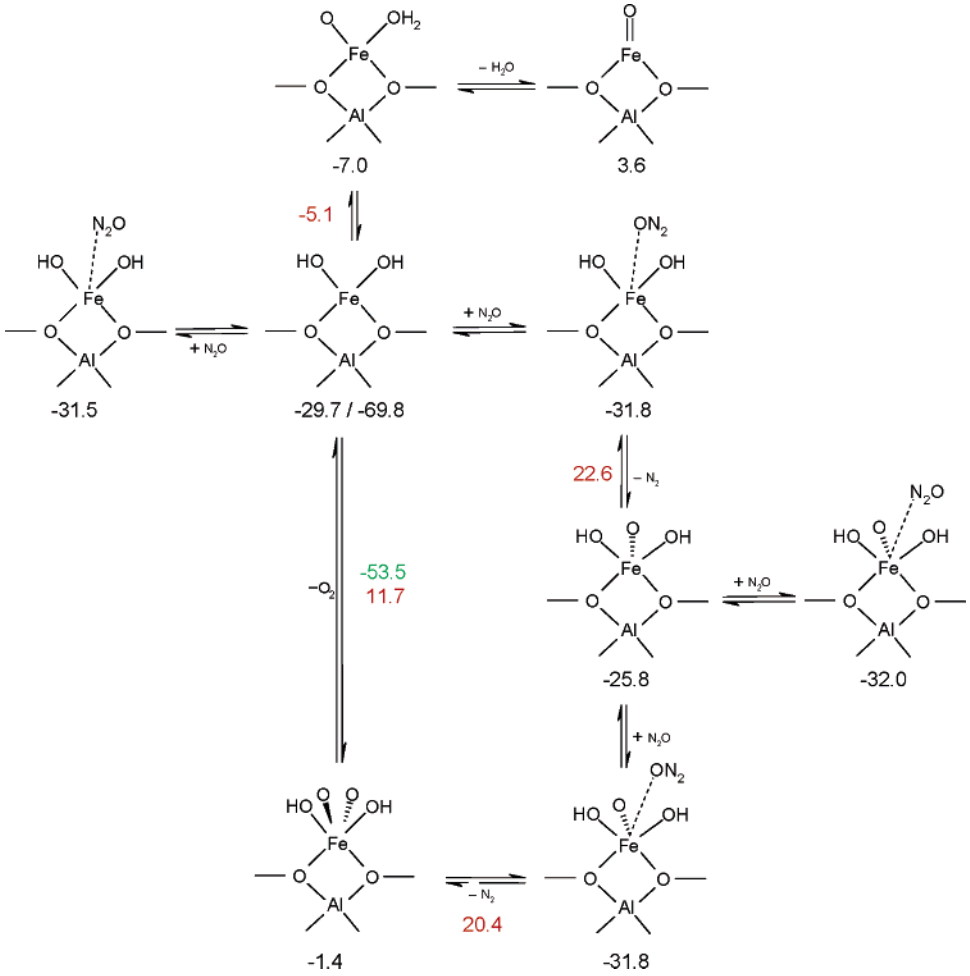

Figure 4. Reaction network of the N_2O dissociation on mononuclear iron hydroxo species. All energies are zero-point corrected, in kcal/mol and with reference to $Z^-[FeO]^+$ $\{M_S = 6\}$ with the appropriate amounts of N_2O, O_2, N_2, H_2O. Energies of potential energy minima are in black. Energies of transition states are in red. Energies of minima on the seam of two PES ($M_S = 4$ and $M_S = 6$) are in green. Structures in black are on the PES with $M_S = 4$.

is on the quartet PES there is no spin change and a transition state for the O_2 desorption can be found. The activation barrier for this reaction is $E^‡ = 11.4$ kcal/mol and the enthalpy change for desorption is $\Delta H_R(M_S = 6) = 1.5$ kcal/mol. The imaginary frequency associated with the transition state mode is $68i$ cm^{-1} ($M_S = 6$). To conclude, owing to the high activation barrier of $E^‡(M_S = 6) = 41.1$ kcal/mol for the second N_2O decomposition reaction and the very fast O_2 desorption possibility on $Z^-[O_2FeO]^+$ sites, $Z^-[FeO_2]^+$ sites are unlikely to be the starting structure for the catalytic cycle for N_2O decomposition on Fe−ZSM-5.

H_2O Adsorption on $Z^-[FeO]^+$. Since $Z^-[FeO]^+$ sites are expected to be essential for the decomposition of N_2O over Fe−ZSM-5, it important to understand how such species might interact with water vapor and whether such an interaction could lead to deactivation of these sites. The interaction of water with $Z^-[FeO]^+$ proceeds via a two step mechanism. First water adsorbs on $Z^-[FeO]^+$ sites and then the adsorbed water dissociate to form a stable iron dihydroxo species, $Z^-[Fe(OH)_2]^+$. As illustrated in Figure 4 for the quartet PES and in Figure 5 for the sextet PES, H_2O adsorption on $Z^-[FeO]^+$ is barrierless and occurs with an enthalpy of adsorption of $\Delta H_{ads}(M_S = 4) = -8.8$ kcal/mol or $\Delta H_{ads}(M_S = 6) = -15.6$ kcal/mol. The Fe−O bond distance of the adsorbed water molecule is 2.25 Å ($M_S = 4$) or 2.15 Å ($M_S = 6$). The transition state for the dissociation of adsorbed H_2O is characterized by a decrease in the Fe−O (from that for H_2O) bond length to 1.98 Å ($M_S = 4$) or 2.04 Å ($M_S = 6$) and an increase in one of the H−O bond lengths from 0.97 Å ($M_S = 4/6$) to 1.18 Å ($M_S = 4$) or 1.20 Å ($M_S = 6$). The H−O distance to the second oxygen atom in the transition state structure is 1.28 Å ($M_S = 4$) or 1.29 Å ($M_S = 6$). Thus, in the transition state, the transferred H atom lies midway between the two surface O atoms. The activation barrier for this reaction is $E^‡(M_S = 4) = 1.9$ kcal/mol or $E^‡(M_S = 6) = 9.2$ kcal/mol, and the imaginary frequency associated with the transition-state mode is $1421i$ cm^{-1} ($M_S = 4$) or $1528i$ cm^{-1} ($M_S = 6$). Since the enthalpy of reaction is $\Delta H_R(M_S = 4) = -23.5$ kcal/mol or $\Delta H_R(M_S = 6) = -27.1$ kcal/mol, the rate of the forward reaction is predicted to be fast and the rate of the reverse reaction to be slow. Further comparison of the electronic energy of a $Z^-[Fe(OH)_2]^+$ site on the quartet and sextet PES shows that the dihydroxo iron species is more stable by 14.9 kcal/mol on the sextet PES than on the quartet PES. Mononuclear iron dihydroxo species exist almost exclusively on the sextet PES. The Fe−OH bond distances in $Z^-[Fe(OH)_2]^+$ are 1.77 Å ($M_S = 4$) or 1.80 Å ($M_S = 6$). The calculated vibrational modes associated with O−H stretches are 3829 and 3836 cm^{-1} on the quartet PES and 3886 and 3891 cm^{-1} on the sextet PES. Consistent with this analysis, EXAFS studies by Choi et al.[27]

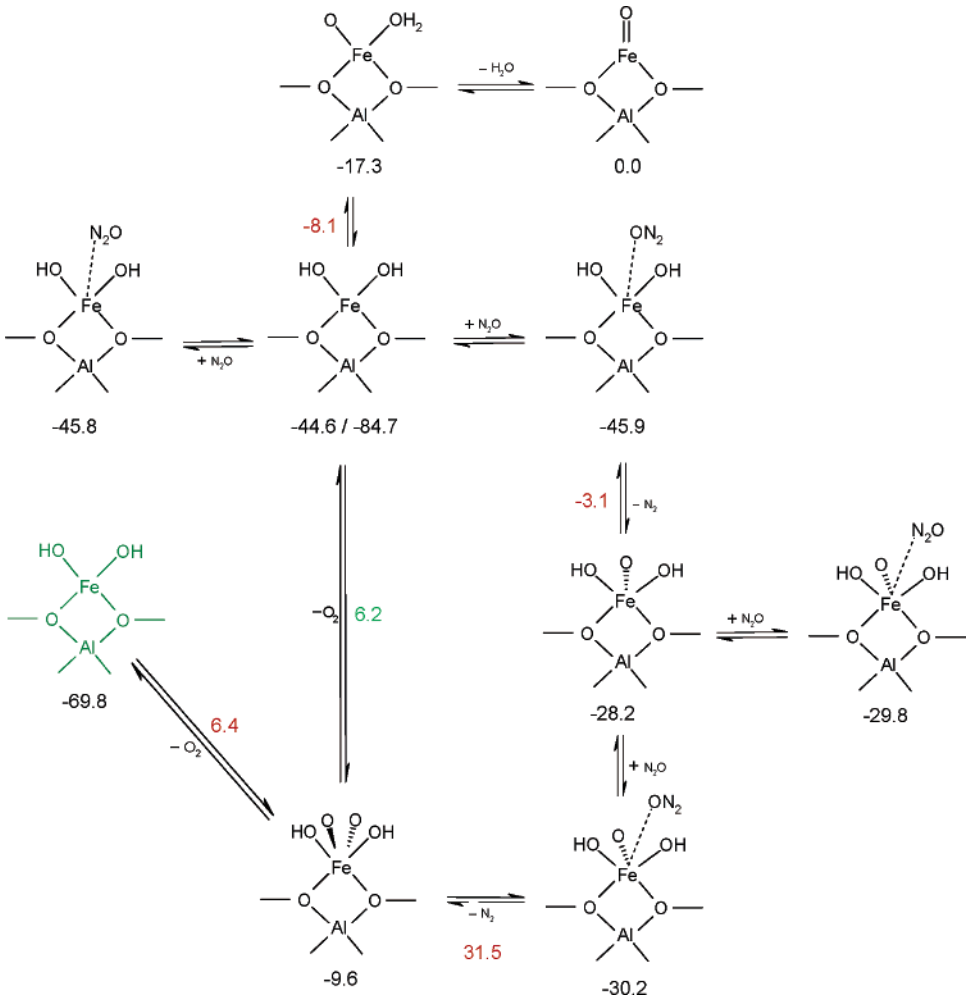

Figure 5. Reaction network of the N_2O dissociation on mononuclear iron hydroxo species. All energies are zero-point corrected, in kcal/mol and with reference to $Z^-[FeO]^+$ {$M_S = 6$} with the appropriate amounts of N_2O, O_2, N_2, H_2O. Energies of potential energy minima are in black. Energies of transition states are in red. Energies of minima on the seam of two PES ($M_S = 6$ and 8) are in green. Structures in black are on the PES with $M_S = 6$. Structures in green are on the PES with $M_S = 4$.

confirm that $Z^-[Fe(OH)_2]^+$ is majority species in Fe−ZSM-5 after pretreatment in He at 573 K.

Catalytic Cycle on $Z^-[Fe(OH)_2]^+$. To assess whether $Z^-[Fe(OH)_2]^+$ species might be involved in N_2O decomposition on Fe−ZSM-5, an analysis of the energetics for this process was carried out. As illustrated in Figures 4 and 5, N_2O adsorbs through the N end with an enthalpy of adsorption of $\Delta H_{ads}(M_S = 4) = -0.2$ kcal/mol or $\Delta H_{ads}(M_S = 6) = 0.4$ kcal/mol. An equally weak adsorption was calculated for N_2O adsorbing through the O end, $\Delta H_{ads}(M_S = 4) = -0.5$ kcal/mol or $\Delta H_{ads}(M_S = 6) = 0.2$ kcal/mol. Thus, hardly any N_2O adsorption is expected on $Z^-[Fe(OH)_2]^+$. Dissociative adsorption of N_2O is possible, but the activation barrier for this process is large. The activation barrier is $E^{\ddagger}(M_S = 4) = 54.4$ kcal/mol or $E^{\ddagger}(M_S = 6) = 42.8$ kcal/mol, and the imaginary frequency associated with the transition-state mode is 583*i* cm^{-1} ($M_S = 4$) or 676*i* cm^{-1} ($M_S = 6$). The major difference between the transition state and the adsorbed state is the bending of the N−N′−O″ bond angle from 180° in the adsorbed state to 161.9°($M_S = 4$) or 154.8°($M_S = 4$) in the transition state. In addition, the N′−O″ bond length increases from 1.20 to 1.74 Å ($M_S = 4$) or 1.61 Å ($M_S = 6$). The reaction is endothermic, with an enthalpy of reaction of $\Delta H_R(M_S = 4) = 5.75$ kcal/mol or $\Delta H_R(M_S = 6) = 16.7$ kcal/mol. In the product state adsorbed O atom is located 1.71 Å ($M_S = 4/6$) from the Fe atom.

In principle, $Z^-[OFe(OH)_2]^+$ species could act as a catalytically active center for N_2O decomposition. N_2O adsorbs through the N end with an enthalpy of adsorption of $\Delta H_{ads}(M_S = 4) = -5.5$ kcal/mol or $\Delta H_{ads}(M_S = 6) = -0.2$ kcal/mol and through the O end the enthalpy of adsorption is $\Delta H_{ads}(M_S = 4) = -5.4$ kcal/mol or $\Delta H_{ads}(M_S = 6) = -0.5$ kcal/mol. The transition state for N_2O dissociation from $Z^-[OFe(OH)_2]^+(ON_2)$ is characterized by a bending of the N_2O molecule from 180° in the adsorbed state to 165.8° ($M_S = 4$) or 160.5° ($M_S = 6$) in the transition state and a lengthening of the N′-O″ bond from 1.20 to 1.70 Å ($M_S = 4$) or 1.85 Å ($M_S = 6$). The activation barrier for N_2O decomposition is $E^{\ddagger}(M_S = 4) = 52.2$ kcal/mol or $E^{\ddagger}(M_S = 6) = 61.7$ kcal/mol and the imaginary frequency associated with the transition state mode is 768*i* cm^{-1} ($M_S = 4$) or 484*i* cm^{-1} ($M_S = 6$). Here too N_2O decomposition is endothermic, with an enthalpy of reaction of $\Delta H_R(M_S = 4) = 30.4$ kcal/mol or $\Delta H_R(M_S = 6) = 19.4$ kcal/mol. Thus, hardly any N_2O is expected to decompose on $Z^-[OFe(OH)_2]^+$.

In $Z^-[O_2Fe(OH)_2]^+$, iron takes on an approximately octahedral coordination. The Fe−O distances of the two surface oxygen species are 1.68−1.71 Å ($M_S = 4$) or 1.79−1.93 Å ($M_S = 6$). The OH-groups are 1.78−2.06 Å ($M_S = 4$) or 1.68−1.74 Å ($M_S = 6$) from the Fe center away. Oxygen can desorb from $Z^-[O_2Fe(OH)_2]^+$. If both the reactant and product states lie on

the sextet PES, the spin-change barrier for desorption is calculated to be 15.8 kcal/mol (sextet/octet PES) and the enthalpy of desorption is calculated to be $\Delta H_R(M_S = 6) = -74.3$ kcal/mol. For the case where the reactant is on the sextet PES and the product is on the quartet PES, there is no spin change, and a transition state for the O_2 desorption can be found. The activation barrier in this case is $E^{\ddagger} = 16.0$ kcal/mol and the enthalpy of desorption is $\Delta H_R(M_S = 6) = -60.2$ kcal/mol. The imaginary frequency associated with the transition state mode (formation of a surface O_2 molecule) is $1076i$ cm^{-1} ($M_S = 6$). When both reactant and product states are on the quartet PES, there is first a transition state for the O_2 formation and then at a significantly lower energy a spin change. The activation barrier for this reaction is therefore determined by the transition state which is $E^{\ddagger} = 13.1$ kcal/mol, and the enthalpy of desorption is $\Delta H_R(M_S = 6) = -68.8$ kcal/mol. The imaginary frequency associated with the transition-state mode is $763i$ cm^{-1} ($M_S = 6$).

In summary, throughout the catalytic cycle for N_2O decomposition on $Z^-[Fe(OH)_2]^+$ the sextet PES is significantly lower in energy than the quartet PES. However, $Z^-[Fe(OH)_2]^+$ species are not candidate site for the N_2O decomposition on Fe−ZSM-5. Both elementary steps involving N_2O dissociation are strongly endothermic and possess significant activation barriers.

Comparison with Experimental Observations. The analysis presented in the preceding sections suggests that $Z^-[FeO]^+$ species could serve as the catalytically active center for N_2O decomposition, as previously proposed by Ryder et al.[35] and Wood et al.[36] The adsorption of water by these species results in the formation of $Z^-[Fe(OH)_2]^+$, which is projected to exhibit very little activity for N_2O decomposition. Consequently, the dehydration of Fe−ZSM-5 is predicted to be an essential step for its activation. This conclusion is supported by the work of Kiwi-Minsker et al.,[11] who showed that an increasing fraction of the Fe in Fe−ZSM-5 becomes active for N_2O decomposition as the temperature and time of catalyst pretreatment in He is raised. These authors also demonstrated that exposure to water vapor of Fe−ZSM-5 originally pretreated at elevated temperature leads to a loss in the fraction of the Fe sites active for N_2O decomposition.

Since the loss of water via dehydration is projected to be a slow process, given the high activation barrier for desorption and the large heat of adsorption for water, it is likely that in most studies of N_2O decomposition over Fe−ZSM-5 reported in the literature the catalyst is only partially dehydrated. Likewise, it is conceivable that the gases used in experimental studies are not totally free of water vapor and that this too could affect the catalyst activity and the apparent rate coefficient. To determine what effect water vapor might have on the apparent activation energy and preexponential factor for N_2O decomposition, we carried out a microkinetic analysis using all 63 elementary reactions listed in Table 1. The temperature of the reactor was then varied, and the logarithm of the apparent first-order rate coefficient (obtained under steady-state conditions) was plotted versus inverse absolute temperature, to determine the apparent activation energy and preexponential factor. Separate calculations confirmed that the rate of N_2O decomposition is first order in N_2O and zero order in O_2 concentration, $r_{N_2O} = -k_{app}P_{N_2O}$, consistent with experimental observation.[1,2,69,70] As noted in Table 3, the presence of water concentrations below 100 ppb has a profound effect on the apparent rate. For example, in the absence of any water vapor, the apparent activation energy is predicted to be 25.5 kcal/mol and the preexponential factor is predicted to be 4.0×10^3 $mol_{N2O}/(s\ mol_{Fe}\ Pa_{N2O})$, whereas in the presence of 100 ppb, the activation energy increases to 54.8 kcal/mol and the preexponential factor increases by 9 orders of magnitude to 6.8×10^{12} $mol_{N2O}/(s\ mol_{Fe}\ Pa_{N2O})$. Since the water content in the gases used for experimental studies is not reported, it is not possible to make a direct comparison between the apparent activation energy predicted using the rate parameters given in Table 1 and those determined from experiments. It is possible to ask, though, what concentration of water vapor would be required to match an experimentally measured value of the apparent activation energy. Comparison was made with the data of Wood et al.,[36] who used a sample of Fe−ZSM-5 for which it had been established by EXAFS that Fe was present as isolated Fe cations. If the water vapor content is assumed to be 23 ppb, then we obtain the same apparent activation energy as that reported by Wood et al.,[36] 44.2 kcal/mol. The apparent preexponential factor measured by these authors is 9.9×10^8 $mol_{N2O}/(s\ mol_{Fe}\ Pa_{N2O})$, whereas that predicted is 3.9×10^9 $mol_{N2O}/(s\ mol_{Fe}\ Pa_{N2O})$. This agreement is quite unanticipated and lends support to our reaction pathway analysis and estimation of rate parameters.

TABLE 3: Experimental and Computed Steady State Rate Parameters for the Overall Reaction Rate Constant of the Nitrous Oxide Decomposition in Fe-ZSM-5[a]

water content (ppb)	activation energy (kcal/mol)	preexponential factor (mol N_2O/s·mol Fe·Pa N_2O)	ref
unknown	44.2	9.9×10^8	36
unknown	32.5	4.4×10^5	9[b]
unknown	36.1	4.4×10^6	9[c]
unknown	44.4	4.7×10^9	9[b,d]
unknown	50.9	2.4×10^{11}	9[c,d]
unknown	46.6	3.5×10^{10}	9[b,e]
unknown	49.0	1.3×10^{11}	9[c,e]
0	25.5	4.0×10^3	this work
1	28.4	3.7×10^4	this work
23	44.2	3.9×10^9	this work
100	54.8	6.8×10^{12}	this work

[a] Computed data are calculated with different amounts of water in reactant stream over the temperature range from 600 to 700 K. [b] Si/Al = 20. [c] Si/Al = 30. [d] High-temperature pretreatment [e] Steam pretreatment.

As a further test of the mechanism and kinetics determined in this study, we compared the activation energies and preexponential factors reported by Zhu et al.[9] for a number of different samples of Fe−ZSM-5. Figure 6 shows that all of the pairs of activation energies and preexponential factors measured by these authors fall along the line predicted on the basis of variations in the concentration of water vapor present in the reactor under steady-state conditions. Also shown for completeness is the data point noted earlier from the work of Wood et al.[36] The remarkable agreement between theory and experiment seen in this figure suggests that the correlation between preexponential factor and activation energy is due primarily to the water vapor content in the reactor. The apparent "compensation relation"[71] observed in Figure 6 is what would be expected if all catalysts, irrespective of water content in the feed or catalyst, achieve an equivalent rate at some temperature, i.e., all Arrhenius plots cross at a single point. From the slope of the line in Figure 6, this temperature is deduced to be 690 K. This means that at 690 K the rate of N_2O decomposition would be expected to be independent of the water content of the reactants because at this temperature only a small fraction of the $Z^-[FeO]^+$ sites will be hydrated, and hence inactive for N_2O decomposition. Below this temperature the water vapor concentration has a significant effect on the apparent rate constant and, consequently,

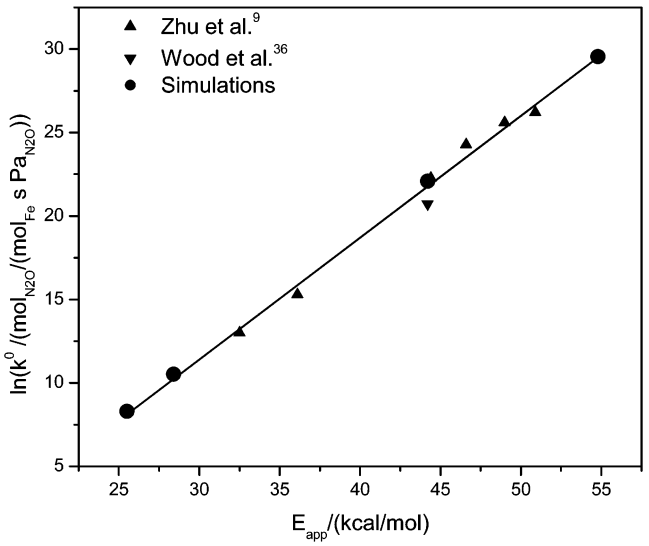

Figure 6. Plot of logarithm of experimental and computed apparent preexponential factor versus apparent activation barrier.

on the apparent preexponential factor and activation barrier obtained experimentally.

The analysis of N_2O decomposition presented here indicates that the rate of molecular oxygen desorption is rapid due to the low activation energy associated with this process, $E^{\ddagger}(M_S = 6/4) = 6.9$ kcal/mol and $E^{\ddagger}(M_S = 6) = 8.0$ kcal/mol. Although this finding is consistent with the experimental observation that N_2O decomposition is not inhibited by the adsorption of O_2, the calculated values of $E^{\ddagger}$ differ from those previously reported on the basis of calculations and determined from temperature-programmed desorption (TPD) studies. Thus, calculations by Ryder et al.[35] based on DFT report a value of $E^{\ddagger} = 51.9$ kcal/mol and TPD studies by Wood et al.[36] and Bulushev et al.[37] give a value of $E^{\ddagger} = 45.7$ kcal/mol. The high value of $E^{\ddagger}$ by Ryder et al.[35] is a consequence of failing to account for the change in spin states occurring during the desorption of O_2 from $Z^-[FeO(O)_2]^+$, as was done in the present study. As will be discussed in a future paper, the values of $E^{\ddagger}$ determined from TPD experiments are attributable to oxygen desorption from $Z^-[FeO_2]^+$, rather than from $Z^-[FeO(O)_2]^+$. In support of this idea, we note that in Table 1 (g and h), the value $E^{\ddagger}$ for the desorption of O_2 from $Z^-[Fe(O)_2]^+$ is calculated to be 50.9 kcal/mol for $M_S = 4$ and 54.2 kcal/mol for $M_S = 6$.

Conclusions

The reaction mechanism of the nitrous oxide decomposition was investigated on hydrated and dehydrated mononuclear iron sites in Fe−ZSM-5 using density functional theory. The most probable catalytic cycle starts on a $Z^-[FeO]^+$ site. The first N_2O decomposition results in $Z^-[FeO_2]^+$ and $Z^-[OFeO]^+$ sites. These are potential structures for the α-oxygen sites in Fe−ZSM-5 and present, therefore, alternative α-oxygen sites to the $Z^-[FeO]^+$ site proposed by Yoshizawa et al.[72] $Z^-[FeO_2]^+$ sites are much more dominant than $Z^-[OFeO]^+$ sites. As suggested by experiment, water adsorbs strongly on $Z^-[FeO]^+$ sites and deactivates these sites. Macroscopic reactor simulations demonstrate that water concentrations in the range of 1−100 ppb have a significant influence on the surface composition and apparent rate coefficients. This is especially relevant in the temperature range from 600 to 700 K where most kinetic studies are performed. Apparent activation barriers determined over this temperature range vary from 28.4 kcal/mol (1 ppb H_2O) to 54.8 kcal/mol (100 ppb H_2O). The catalyst surface changes dramatically with temperature if traces of water are present. At 600 K, the surface is covered with $Z^-[Fe(OH)_2]^+$ sites and hardly any active $Z^-[FeO]^+$ or $Z^-[FeO_2]^+$ sites are present. At 700 K, water desorbs from $Z^-[Fe(OH)_2]^+$ sites, and $Z^-[FeO]^+$ and $Z^-[FeO_2]^+$ sites then form the majority surface species. It was possible to match the experimental activation barrier from Wood et al.[36] of 44.2 kcal/mol with a water content of 23 ppb in the He stream. The preexponential factor is in this case 3.9×10^9 $mol_{N2O}/(s\ mol_{Fe}\ Pa_{N2O})$. The calculated preexponential factor is approximately a factor four larger than the experimental one. This level of agreement is remarkable, considering all of the approximations existent in the theoretical methods used to calculate the rate parameters for each elementary reaction. Finally, it can be concluded that the spread in the values of the rate parameters reported by different research groups is likely a reflection of the influence of water impurities.

Acknowledgment. The authors appreciate helpful discussions with Professor Arup K. Chakraborty. The authors thank Dr. Jens Döbler and Dr. Bernd Kallies for support with the TURBOMOLE V5.6 software package. Computations were carried out at the "Norddeutscher Verbund für Hoch- und Höchstleistungsrechnen" (HLRN)[73] on an IBM p690-Cluster. This work was supported by the Methane Conversion Cooperative funded by B.P., the "Fonds der chemischen Industrie", and the Max-Buchner-Forschungsstiftung.

Note Added after Print Publication. Figures 2−5 should have been printed in color when this manuscript was published on the Web on January 19, 2005 (ASAP) and in the print version (Vol. 109, No. 5, February 3, p 1857). The electronic version of the manuscript was corrected on February 25, 2005, and an Addition and Correction appears in the March 17, 2005 issue (Vol. 109, No. 10).

References and Notes

(1) Panov, G- I.; Sobolev, V. I.; Kharitonov, A. S. *J. Mol. Catal.* **1990**, *61*, 85.
(2) Kapteijn, F.; Marbán, G.; Rodriguez-Mirasol, J.; Moulijn, J. A. *J. Catal.* **1997**, *167*, 256.
(3) Panov, G. I.; Uriarte, A. K.; Rodkin, M. A.; Sobolev, V. I. *Catal. Today* **1998**, *41*, 365.
(4) Sang, C.; Lund, C. R. F. *Catal. Lett.* **2000**, *70*, 165.
(5) El-Malki, E. M.; van Santen, R. A.; Sachtler, W. M. H. *Microporous Mater.* **2000**, *35*−*36*, 235.
(6) El-Malki, E. M.; van Santen, R. A.; Sachtler, W. M. H. *J. Catal.* **2000**, *196*, 212.
(7) Sang, C.; Lund, C. R. F. *Catal. Lett.* **2001**, *73*, 73.
(8) Wood. B. R.; Reimer, J. A.; Bell, A. T. *J. Catal.* **2002**, *209*, 151.
(9) Zhu, Q.; Mojet, B. L.; Janssen, R. A. J.; Hensen, E. J. M.; van Grondelle, J.; Magusin, P. C. M. M.; van Santen, R. A. *Catal. Lett.* **2002**, *81*, 205.
(10) Pérez-Ramírez, J.; Kapteijn, F.; Groen, J. C.; Doménech, A.; Mul, G.; Moulijn, J. A. *J. Catal.* **2003**, *214*, 33.
(11) Kiwi-Minsker, L.; Bulushev, D. A.; Renken, A. *J. Catal.* **2003**, *219*, 273.
(12) Joyner, R.; Stockenhuber, M. *J. Phys. Chem. B* **1999**, *103*, 5963.
(13) Hensen, E. J. M.; Zhu, Q.; Hendrix, M. M. R. M.; Overweg, A. R.; Kooyman, P. J.; Sychev, M. V.; van Santen, R. A. *J. Catal.* **2004**, *221*, 560.
(14) Zhu, Q.; van Teeffelen, R. M.; van Santen, R. A.; Hensen, E. J. M. *J. Catal.* **2004**, *221*, 575.
(15) Battiston, A. A.; Bitter, J. H.; Koningsberger, D. C. *Catal. Lett.* **2000**, *66*, 75.
(16) Battiston, A. A.; Bitter, J. H.; de Groot, F. M. F.; Overweg, A. R.; Stephan, O.; van Bokhoven, J. A.; Kooyman, P. J.; van der Spek, C.; Vankó, G.; Koningsberger, D. C. *J. Catal.* **2003**, *213*, 251.
(17) Battiston, A. A.; Bitter, J. H.; Heijboer, W. M.; de Groot, F. M. F.; Koningsberger, D. C. *J. Catal.* **2003**, *215*, 279.

(18) Battiston, A. A.; Bitter, J. H.; Koningsberger, D. C. *J. Catal.* **2003**, *218*, 163.
(19) Marturano, P.; Drozdová, L.; Kogelbauer, A.; Prins, R. *J. Catal.* **2000**, *192*, 236.
(20) Marturano, P.; Drozdová, L.; Pirngruber, G. D.; Kogelbauer, A.; Prins, R. *Phys. Chem. Chem. Phys.* **2001**, *3*, 5585.
(21) Jia, J.; Sun, Q.; Wen, B.; Chen, L. X.; Sachtler, W. M. H. *Catal. Lett.* **2002**, *82*, 7.
(22) Dubkov, K. A.; Ovanesyan, N. S.; Shteinman, A. A.; Starokon, E. V.; Panov, G. I. *J. Catal.* **2002**, *207*, 341.
(23) Pérez-Ramírez, J.; Mul, G.; Kapteijn, F.; Moulijn, J. A.; Overweg, A. R.; Doménech, A.; Ribera, A.; Arends, I. W. C. E. *J. Catal.* **2002**, *207*, 113.
(24) Overweg, A. R.; Crajé, M. W. J.; van der Kraan, A. M.; Arends, I. W. C. E.; Ribera, A.; Sheldon, R. A. *J. Catal.* **2004**, *223*, 262.
(25) Lobree, L. J.; Hwang, I. C.; Reimer, J. A.; Bell, A. T. *J. Catal.* **1999**, *186*, 242.
(26) Kucherov, A. V.; Shelef, M. *J. Catal.* **2000**, *195*, 106.
(27) Choi, S. H.; Wood, B. R.; Ryder, J. A.; Bell, A. T. *J. Phys. Chem. B* **2003**, *107*, 11843.
(28) Choi, S. H.; Wood, B. R.; Bell, A. T.; Janicke, M. T.; Ott, K. C. *J. Phys. Chem. B* **2004**, *108*, 8970.
(29) Pérez-Ramírez, J.; Kumar, M. S.; Brückner, A. *J. Catal.* **2004**, *223*, 13.
(30) Yakovlev, A. L.; Zhidomirov, G. M.; van Santen, R. A. *Catal. Lett.* **2001**, *75*, 45.
(31) Kachurovskaya, N. A.; Zhidomirov, G. M.; Hensen, E. J. M.; van Santen, R. A. *Catal. Lett.* **2003**, *86*, 25.
(32) Yakovlev, A. L.; Zhidomirov, G. M.; van Santen, R. A. *J. Phys. Chem. B* **2001**, *105*, 12297.
(33) Yoshizawa, K.; Yumura, T.; Shiota, Y.; Yamabe, T. *Bull. Chem. Soc. Jpn.* **2000**, *73*, 29.
(34) Yoshizawa, K.; Shiota, Y.; Yumura, T.; Yamabe, T. *J. Phys. Chem. B* **2000**, *104*, 734.
(35) Ryder, J. A.; Chakraborty, A. K.; Bell, A. T. *J. Phys. Chem. B* **2002**, *106*, 7059.
(36) Wood, B. R.; Reimer, J. A.; Bell, A. T.; Janicke, M. T.; Ott, K. C. *J. Catal.* **2004**, *224*, 148.
(37) Bulushev, D. A.; Kiwi-Minsker, L.; Renken, A. *J. Catal.* **2004**, *222*, 389.
(38) Yoshizawa, K.; Shiota, Y.; Yamabe, T. *J. Chem. Phys.* **1999**, *111*, 538.
(39) Shaik, S.; Danovich, D.; Fiedler, A.; Schröder, D.; Schwarz, H. *Helv. Chim. Acta* **1995**, *78*, 1393.
(40) Shaik, S.; Filatov, M.; Schröder, D.; Schwarz, H. *Chem. Eur. J.* **1998**, *4*, 193.
(41) Danovich, D.; Shaik, S. *J. Am. Chem. Soc.* **1997**, *119*, 1773.
(42) Powell, M. J. D. A method for nonlinear constraints in minimization problems. In *Optimization*; Fletcher, R., Ed.; Academic Press: London, 1969.
(43) Peters, B.; Heyden, A.; Bell, A. T.; Chakraborty, A. *J. Chem. Phys.* **2004**, *120*, 7877.
(44) Heyden, A.; Bell, A. T.; Keil, F. J. *J. Chem. Phys.* submitted.
(45) Olson, D. H.; Kokotallo, G. T.; Lawton, S. L.; Meier, W. M. *J. Phys. Chem.* **1981**, *85*, 2238.
(46) Parr, R. G.; Yang, W. *Density Functional Theory of Atoms and Molecules;* Oxford University Press: Oxford, U.K., 1989.
(47) Becke, A. D. *Phys. Rev. A* **1988**, *38*, 3098.
(48) Lee, C.; Yang, W.; Parr, R. G. *Phys. Rev. B* **1988**, *37*, 785.
(49) Schäfer, A.; Huber, C.; Ahlrichs, R. *J. Chem. Phys.* **1994**, *100*, 5829.
(50) Kestner, N. R.; Combariza, J. E. In *Reviews in Computational Chemsitry*; Lipkowitz, K. B., Boyd, D. B., Eds.; John Wiley and Sons: New York, 1999; Vol. 13, Chapter 2.
(51) Ahlrichs, R.; Bär, M.; Häser, M.; Horn, H.; Kölmel, C. *Chem. Phys. Lett.* **1989**, *162*, 165.
(52) Ahlrichs, R.; v. Armin, M. In *Methods and Techniques in Computational Chemistry: METECC-95*; Clementi, E., Corongiu, G., Eds.; STEF: Calgari, 1995.
(53) Zilberberg, I.; Gora, R. W.; Zhidomirov, G. M.; Leszczynski, J. *J. Chem. Phys.* **2002**, *117*, 7153.
(54) http://www.Gaussian.com/g_whitepap/vib.html.
(55) Henkelman, G.; Jonsson, H. *J. Chem. Phys.* **2000**, *113*, 9978.
(56) Mills, G.; Jonsson, H. *Phys. Rev. Lett.* **1994**, *72*, 1124.
(57) Ren, W. *Numerical methods for the Study of Energy Landscapes and rare events*. Ph.D. Thesis, New York University, 2002.
(58) Fletcher, R. *Practical Methods of Optimization*, 2nd ed.; John Wiley & Sons: New York, 1987.
(59) McQuarrie, D. A. *Statistical Mechanics*; Harper Collins Publisher Inc.: New York, 1973.
(60) Laidler, K. J. *Chemical Kinetics*, 3rd ed.; Harper & Row Publisher: New York, 1987; p 263.
(61) Zener, C. *Proc. R. Soc.* **1932**, *A137*, 696.
(62) Zener, C. *Proc. R. Soc., A* **1933**, *140*, 660.
(63) Landau, L. *Physik. Zeits. Sowjetunion* **1932**, *2*, 46.
(64) Stearn, A. E.; Eyring, H. *J. Chem. Phys.* **1935**, *3*, 778.
(65) Danovich, D.; Shaik, S. *J. Am. Chem. Soc.* **1997**, *119*, 1773.
(66) Chen, H.-Y.; El-Malki, El-M.; Wang, X.; van Santen, R. A.; Sachtler, W. M. H. *J. Mol. Catal. A* **2000**, *162*, 159.
(67) Gao, Z.-X.; Kim, H.-S.; Sun, Q.; Stair, P. C.; Sachtler, W. M. H. *J. Phys. Chem. B* **2001**, *105*, 6186.
(68) Che, M.; Tench, A. J. *Adv. Catal.* **1983**, *32*, 1.
(69) Fu, C. M.; Korchak, V. N.; Hall, W. K. *J. Catal.* **1981**, *68*, 166.
(70) Leglise, J.; Petunchi, J. O.; Hall, W. K. *J. Catal.* **1984**, *86*, 392.
(71) Bond, G. C.; Kaene, M. A.; Kral, H.; Lercher, J. A. *Catal. Rev.-Sci. Eng.* **2000**, *42* (3), 323.
(72) Yoshizawa, K.; Shiota, Y.; Kamachi, T. *J. Phys. Chem. B* **2003**, *107*, 11404.
(73) http://www.hlrn.de.